nature communications

Article

https://doi.org/10.1038/s41467-026-70062-6

A microbiota-IPA axis facilitates intestinal stem cell-mediated regeneration in colitis through a *Hopx*-associated program

Received: 13 October 2025

Accepted: 16 February 2026

Published online: 25 February 2026

Check for updates

Yanan Zhang[1,5], Jinxin Meng[1,5], Shuyu Tu[1,2,5], Linlin Ma[3,5], Xinya Zhao[1], Jinsong Gao[4], Jianan Wu[1], Weilv Xu[1], Shuxian Chen[1], Hairong Cheng[3] ✉, Li Zhang[2] ✉ & Shu Jeffrey Zhu[1,4] ✉

The gut microbiota plays a crucial role in maintaining intestinal stem cell (ISC) homeostasis and epithelial barrier integrity. Here, we report that *Blautia coccoides* (*B. coccoides*) is significantly reduced in inflammatory bowel disease (IBD) patients and dextran sulfate sodium (DSS)-induced colitis mice. Through an integrated approach combining RNA sequencing, metabolomic profiling, and ISC lineage tracing across multiple mucosal injury models, we demonstrate that *B. coccoides* colonization enhances β-hydroxybutyrate (BHB) production in intestinal epithelial cells (IECs), which activates HOPX$^+$ reserve ISCs and promotes regeneration of the LGR5$^+$ ISC pool, thereby accelerating epithelial repair. We further show that *B. coccoides*-derived indole-3-lactic acid (ILA), a tryptophan (Trp) metabolite, is converted into indole-3-propionic acid (IPA) by commensal bacteria such as *P. russellii* or *C. sporogenes*, stimulating IEC BHB synthesis. Using an engineered *Escherichia coli* strain expressing BC-derived phenyllactate dehydrogenase (*fldH*), we establish that both dietary Trp and bacterial fldH activity are essential for ILA/IPA generation and subsequent mucosal healing. Our findings reveal a microbiota-metabolite-ISC regulatory axis critical for epithelial regeneration and propose novel metabolite-based therapeutic strategies for IBD and other intestinal disorders associated with barrier dysfunction.

The intestinal epithelium constitutes an essential interface that segregates luminal material from the underlying stromal environment. Preservation of this barrier is crucial, as its compromise, whether resulting from infection, inflammatory pathology, or clinical procedures, can lead to exposure of the host to otherwise confined luminal antigens and pathogens. Following significant epithelial damage, such as crypt loss associated with inflammatory bowel disease (IBD), intestinal stem cells (ISCs) become activated to drive robust proliferation and differentiation, thereby replenishing the epithelial compartment and facilitating mucosal healing post-injury[1,2]. Dysregulated or impaired ISC function has emerged as a key factor in the pathogenesis of IBD, a concept increasingly supported by recent investigations[3–5].

Intestinal epithelial homeostasis relies on two distinct types of stem cells that drive epithelial turnover: active ISCs (aISCs), which are

[1]Department of Veterinary Medicine, College of Animal Sciences, Zhejiang University, Hangzhou, Zhejiang, China. [2]Department of Cardiology, The First Affiliated Hospital of Guangdong Pharmaceutical University, Guangzhou, Guangdong, China. [3]Engineering Research Center of Glycoconjugates, Ministry of Education, Jilin Provincial Key Laboratory of Chemistry and Biology of Changbai Mountain Natural Drugs, School of Life Sciences, Northeast Normal University, Changchun, China. [4]Department of Critical Care Medicine, Sir Run Run Shaw Hospital, Zhejiang University School of Medicine, Hangzhou, China. [5]These authors contributed equally: Yanan Zhang, Jinxin Meng, Shuyu Tu, Linlin Ma. ✉e-mail: chenghr893@nenu.edu.cn; Zhangli4029@126.com; shuzhu@zju.edu.cn

fast-cycling crypt base columnar (CBC) cells characterized by the expression of *Lgr5*[2]; and reserve ISCs (rISCs), a cohort of quiescent, slow-cycling "+4" stem cells marked by expression of *Hopx*, *Lrig1*, *Tert*, and *Bmi1*[6–9]. Although LGR5$^+$ aISCs are integral to routine intestinal homeostasis, they are susceptible to damage[10,11]. In contrast, HOPX$^+$ rISCs display enhanced resilience and play a supportive role in the intestinal lineage during the regenerative phase[12,13]. Although lineage tracing and cell ablation studies have shown that a specific rISC subset characterized by high clusterin (*Clu*) expression can restore the LGR5$^+$ aISC population and support intestinal epithelium regeneration[14], the nature of the functional regenerative stem cell pool in colitis-associated repair has been elusive.

Investigations employing germ-free (GF) mouse models have demonstrated a marked reduction in the turnover and regenerative capacity of intestinal epithelial cells (IECs) following injury[15], highlighting the pivotal role of gut microbiota and their metabolic products in promoting tissue recovery after intestinal damage. While there is growing recognition of the influence of microbial metabolites on the ISC niche and mucosal barrier integrity[16,17], the detailed mechanisms connecting ISC activity to microbiota-derived signals remain incompletely elucidated. Moreover, the particular commensal bacterial species that modulate ISC stemness, plasticity, and behavioral dynamics remain to be fully characterized.

Here, through comparative analysis of the intestinal microbiome from IBD patients and DSS-induced colitis mice, we identified a significant reduction in *Blautia coccoides* (hereafter referred to as BC) in both diseased cohorts. Utilizing an integrated approach comprising RNA sequencing (RNA-seq), metabolomic profiling, lineage tracing of ISCs, and multiple mucosal injury models, we demonstrate that BC colonization enhances β-hydroxybutyrate (BHB) production within IECs. This elevation in BHB promotes the activation of HOPX$^+$ rISCs, leading to reconstitution of the LGR5$^+$ aISC pool and accelerating epithelial repair following mucosal damage.

Notably, we found that the tryptophan (Trp)-derived microbial metabolite indole-3-lactic acid (ILA), produced by BC, serves as a precursor that is further metabolized into indole-3-propionic acid (IPA) by *Peptostreptococcus russellii* (*P. russellii*) or *Clostridium sporogenes* (*C. sporogenes*), thereby facilitating BHB synthesis in IECs. By employing an engineered *Escherichia coli* (*E. coli*) strain carrying the BC-derived phenyllactate dehydrogenase (*fldH*) gene, we further established that both dietary Trp and bacterial fldH enzymatic activity are indispensable for ILA generation in the gut. Ultimately, this BC-dependent metabolic pathway contributes to IPA production and promotes mucosal healing in experimental IBD.

Results

The abundance of BC is decreased in human and mice with colitis

Given that gut microbial dysbiosis is a hallmark of IBD[18,19], we first profiled microbiota alterations potentially driving IBD pathogenesis. Comparative 16S rRNA sequencing of fecal samples from 28 healthy controls and 32 Crohn's disease (CD) patients revealed significantly enriched *Blautia* spp. in non-IBD individuals (Fig. 1a, b, and Supplementary Fig. 1a). This finding was validated in public metagenomic datasets, where *Blautia* abundance remained substantially higher in non-IBD controls versus CD cohorts (Fig. 1c). BC, a key SCFA-producing strain implicated in barrier fortification[20,21], showed marked depletion in IBD patients, particularly CD cases (Fig. 1d, e). Although two independent Chinese cohorts exhibited consistent downward trends in BC abundance among ulcerative colitis (UC) and CD patients relative to controls, statistical significance was not reached (Fig. 1f, g). Mirroring human observations, BC abundance declined significantly in DSS-induced murine colitis (Fig. 1h and Supplementary Fig. 1b-i).

BC ameliorates intestinal inflammation by restoring the mucosal barrier functions in multiple colitic mouse models

To define the protective role of BC in IBD, we subjected wild-type C57BL/6J mice (WT B6) to DSS-induced colitis following dual colonization with BC (10^9 CFU) following previous work[22]. *Enterococcus faecalis* (EF), which causes nosocomial infection in hospitalized patients, served as an unrelated Gram-positive commensal bacterial control. BC stably colonized in the gut of treated animals (Supplementary Fig. 1b-ii, c) and conferred significant protection against colitis, as evidenced by attenuated disease severity including preserved colon length (Fig. 1i, and Supplementary Fig. 1d), reduced histopathological damage (Fig. 1j, k), and diminished infiltration of IL-6$^+$ macrophages at D7 post-challenge. In contrast, EF-colonized mice exhibited pathology comparable to vehicle (Veh) controls. BC administration further suppressed colonic proinflammatory cytokines (IL-1β, IL-6, TNF-α) at transcriptional and translational levels relative to EF- or vehicle-colonized groups (Fig.1k, l and Supplementary Fig. 1e).

We next extended our findings to a TNBS-induced model of persistent chemical injury (Supplementary Fig. 1b-iii), where BC colonization significantly ameliorated both colon shortening and histopathological changes (Fig. 1m–o, and Supplementary Fig. 1d).

Given the persistent inflammatory stimuli inherent to DSS colitis models, we employed a radiation enteritis (RE) model, featuring discrete, single-dose abdominal irradiation (16 Gy) to confirm the protective role of BC in transient injury contexts (Supplementary 1b-iv). Consistent with the results observed in DSS-induced models, BC colonization conferred protection at D7 post radiation, reflected by attenuated histopathological damage, elevated tight junction proteins and *Muc2* expression, and suppressed *Tnfa* levels (Fig. 1p, q, and Supplementary Fig. 1f–h).

To define the enhancing effect exerted by BC on mucosal wound healing during the regenerative process, we administered BC to WT B6 mice immediately following DSS cessation. BC-colonized animals exhibited accelerated mucosal repair, manifesting as attenuated colonic shortening alongside significant reductions in histopathological damage and apoptotic events relative to Veh-treated controls (Fig. 1r–t, and Supplementary Fig. 1b-v).

Given the established synergy between epithelial barrier failure and dysregulated immunity in IBD pathogenesis[5,23], we examined the influence of BC on mucosal integrity. BC enhanced barrier function in the colon through increased goblet cell numbers and upregulated expression of tight junction proteins (ZO-1, occludin) and Muc2, whereas EF colonization provided no such benefit (Fig. 1k, u). Notably, flow cytometric analysis revealed no significant alterations in key colonic lamina propria immune cell populations, including leukocytes (macrophages, dendritic cells, and neutrophils) and lymphocytes (CD4$^+$ and CD8$^+$ T cells), either at baseline or D7 post-injury (Supplementary Fig. 1i). These collective observations indicate that BC-mediated protection operates primarily through restoration of epithelial barrier competence rather than broad recalibration of mucosal immunity.

BC colonization rescues the loss of LGR5$^+$ ISCs and promotes epithelial regeneration

To delineate the mechanisms underlying BC-mediated barrier enhancement, we performed RNA sequencing (RNA-seq) of bulk colonic intestinal epithelial cells (cIECs) isolated from BC-colonized and control mice at D0, D3, and D7 post-DSS challenge (Fig. 2a). GO and Kyoto Encyclopedia of Genes and Genomes (KEGG) pathway enrichment analysis of BC-upregulated genes at D7 revealed significant enrichment in pathways critical for ISC niche maintenance and barrier integrity, including Bone Morphogenetic Protein (BMP) regulation, Wnt signaling, and tight junction (Fig. 2b). Transcriptional profiling further showed that BC colonization increased expression of the rISC marker *Hopx* even at D0, while markers of aISCs (*Lgr5*/*Ascl2*) and

https://doi.org/10.1038/s41467-026-70062-6

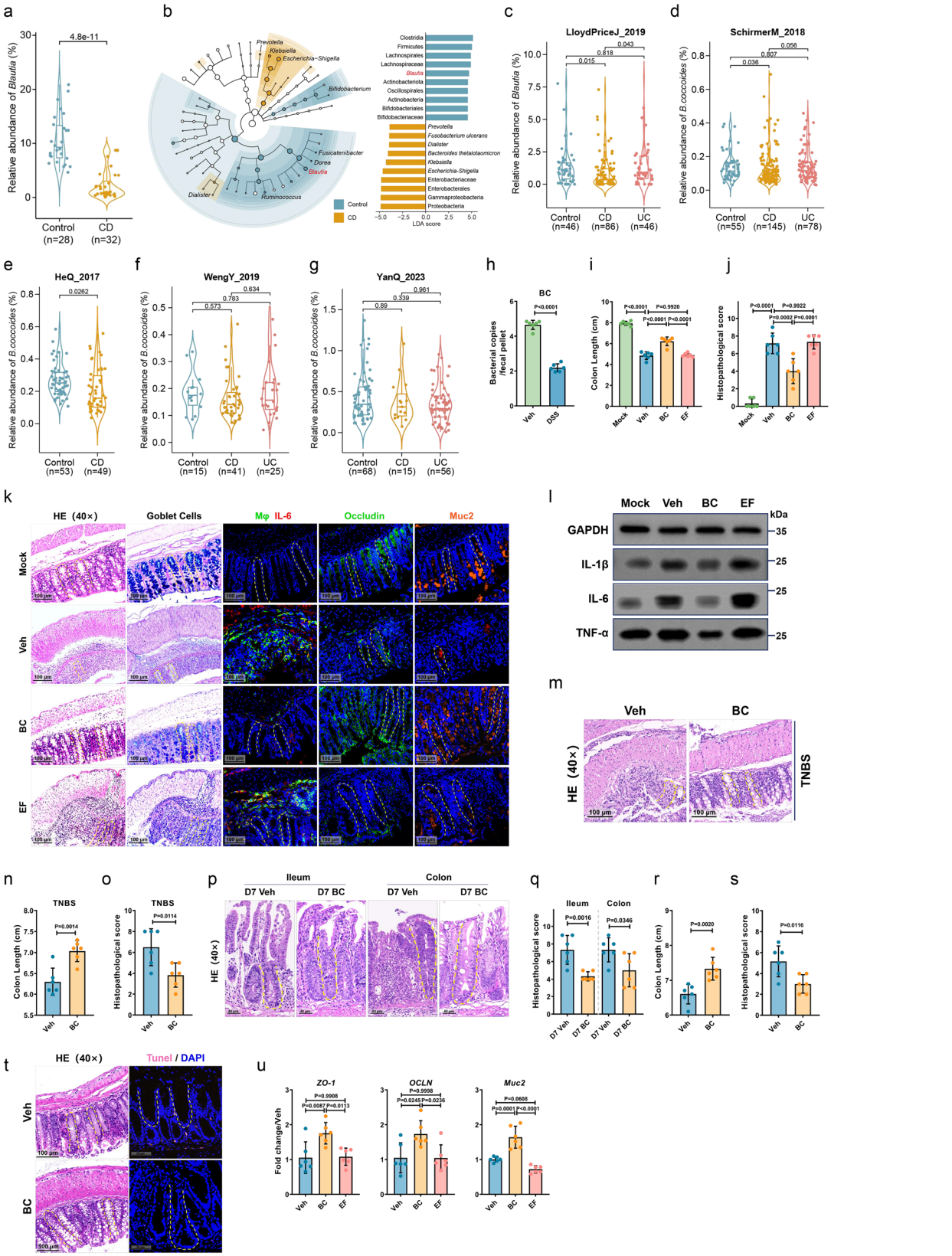

secretory lineages (*Ang4*/*Lyz1* for Paneth cells; *Dclk1*/*Cd24a*/*Trpm5* for Tuft cells) were significantly amplified only at D3 and D7 post-DSS (Fig. 2c–e). This BC-dependent transcriptional program was validated by qPCR showing elevated *Lgr5*, *Hopx*, *Muc2*, and *Clu* expression in cIECs at D7 (Fig. 2f).

Immunofluorescence analysis (IFA) corroborated that BC colonization preserved LGR5^{+} ISCs in crypt compartments and enhanced Ki-67^{+} proliferation at D7 post-injury, whereas Veh-treated controls exhibited profound ISC loss. Importantly, no differences in epithelial proliferation were observed at homeostasis (D0) (Fig. 2g, h).

Fig. 1 | *B. coccoides* ameliorates intestinal inflammation by restoring the mucosal barrier functions in multiple colitic mouse models. a Violin plots overlaid with boxplots show the relative abundance of *Blautia* in fecal samples from healthy individuals ($n = 28$) and patients with Crohn's disease (CD, $n = 32$). The width of each violin represents the kernel density estimation of the data distribution. Boxes indicate the interquartile range (IQR), center lines indicate medians, and whiskers extend to values within 1.5× the IQR. Dots represent outlier samples beyond the whiskers. Individual points represent single samples. **b** Linear discriminant analysis (LDA) effect size (LEfSe) analysis identifying key microbial features distinguishing CD patients ($n = 32$) from healthy controls ($n = 28$). Violin plots show the relative abundance of *Blautia* (**c**, amplicon-based metagenomics) and *B. coccoides* (BC; **d**–**g**, shotgun metagenomics) in the gut microbiota of publicly available cohorts of patients with inflammatory bowel disease (IBD) and healthy controls. Plot characteristics are as described in (**a**). **h** BC genomic copies in feces from WT mice with or without DSS induction ($n = 6$). WT-DSS model colonized with Veh/BC/EF ($n = 6$): D7 phenotypes (**i**–**k**); Western blot of IL-1β, IL-6, TNF-α (**l**). TNBS-colitis model ($n = 6$): HE-stained sections (**m**), colon length (**n**) and histology (**o**). **p**, **q** ileal and colonic histopathology in radiation enteritis model (16 Gy IR, $n = 6$). Therapeutic BC post-DSS ($n = 6$): (**r**, **s**) Colon length and histopathology; (**t**) Tissue damages and TUNEL staining post-DSS recovery. **u** *OCLN*, *ZO-1*, *Muc2* in cIECs at D7 post-DSS ($n = 6$). For (**a**, **c**–**g**) statistical significance was assessed using two-sided Wilcoxon rank-sum tests, following by Benjamini–Hochberg (BH) correction for multiple comparisons when a cohort contained ≥3 groups. Other statistical significance determined using two-sided Student's *t*-test or one-way ANOVA followed by Tukey's post hoc test for multiple comparisons. Data represent mean ± SD from ≥2 independent experiments. Source data are provided as a Source Data file.

We next assessed the functional impact of BC colonization on regeneration using ex vivo organoids. Colon crypts from uninjured (D0) mice formed organoids equivalently regardless of BC status, confirming negligible baseline effects. On the contrary, crypts from Veh-treated colitic mice (D3) showed minimal expansion and pronounced degeneration, whereas BC-colonized counterparts retained robust organoid-forming capacity with reduced cell death (Fig. 2i–k). Collectively, these data establish that BC restores epithelial regeneration by replenishing injury-depleted LGR5$^+$ ISCs under inflammatory duress.

BC induces HOPX$^+$ rISCs to reconstitute depleted LGR5$^+$ ISCs following acute mucosal injury

To investigate the mechanism whereby BC promotes ISC proliferation, our RNA-seq analysis of cIECs revealed consistent upregulation of *Hopx*, the marker of rISCs in BC-colonized mice across all post-DSS timepoints (Fig. 2c–e). This finding aligns with previous work identifying HOPX$^+$ colitis-associated regenerative stem cells, a population characterized by rapid proliferative capacity and fetal-like marker expression that orchestrates mucosal healing in DSS-induced colitis[12]. Given established evidence that CLU$^+$ rISCs can reconstitute the LGR5$^+$ CBC compartments[14], we hypothesize that BC mobilizes HOPX$^+$ rISCs to regenerate LGR5$^+$ aISCs ablated during inflammatory injury.

To test our hypothesis, we first delineated the temporal dynamics of *Hopx* and *Lgr5* expression in cIECs. BC colonization consistently amplified *Hopx* transcripts across all post-injury timepoints (Fig. 3a, and Supplementary Fig. 2a–i), while inducing a transient suppression of *Lgr5* at days D0 and D1 followed by significant induction at D3 and D7 versus Veh controls (Fig. 3b).

IFA analysis indicated that Veh-treated mice exhibited rapid depletion of LGR5$^+$ ISCs with concurrent expansion of HOPX$^+$ rISCs during early injury (D1 and D3), suggesting immediate rISC activation. At D7 post injury, however, these controls showed near-complete collapse of both ISC pools alongside crypt atrophy, consistent with failed regeneration as reported by Wang et al.[12]. Critically, BC colonized mice maintained expanded HOPX$^+$ and LGR5$^+$ compartments through day 7, demonstrating sustained regenerative capacity (Fig. 3c–e).

To further confirm the phenotype, we utilized the *Hopx-Cre^{ERT2}*; H11-*CAG-LSL-tdTomato* mice (*Hopx* lineage tracer, termed as *Hopx^{CreER}*/H11^{Td}) to transiently label HOPX$^+$ rISCs by tamoxifen (TAM) induction (Supplementary Fig. 2a-ii). In BC-colonized colitic *Hopx^{CreER}*/H11^{Td} mice, there were significantly increased numbers of HOPX$^+$ daughter cells with LGR5 staining in the crypt compartments at D3 post-DSS administration (Fig. 3f), which suggests that BC-induced HOPX$^+$ cells give rise to a de novo population of LGR5$^+$ ISCs during DSS-induced epithelium injury.

Yes-associated protein 1 (YAP-1), a transcriptional regulator inhibited by Hippo signaling, is required for reconstitution of LGR5$^+$ CBCs from rISCs in the intestinal epithelium during wound healing[14,24]. Consistent with the *Lgr5*/*Hopx* kinetics and IFA results, there was a significantly elevated expression of YAP1 in the colon crypts of BC-colonized mice compared with Veh-treated controls at D3 post-DSS administration (Fig. 3g, and Supplementary Fig. 2b).

Leveraging the RE model to assess transient injury responses, we observed that BC colonization greatly induced *Lgr5*, *Hopx* and *Yap1* expression in ileal crypts at D3 post-16Gy irradiation (Fig. 3h–j, and Supplementary Fig. 2a-iii). This pro-regenerative signature paralleled in colonic crypts, though significant *Hopx* upregulation mediated by BC colonization (Supplementary Fig. 2c–e).

Lastly, BC enforced expression of the *Lgr5*, *Hopx* and *Yap1* and increased the LGR5$^+$ and HOPX$^+$ cells in the colon crypts in the BC therapeutic model (Fig. 3k–m, and Supplementary Fig. 2a-iv), further supporting the paradigm that BC promotes LGR5$^+$ ISC proliferation in response to intestinal epithelium injury through HOPX$^+$ rISC activation in the absence of DSS.

BC and BHB compensate for LGR5$^+$ ISC depletion to restore intestinal epithelium regeneration through HOPX

Having observed that BC promotes rISC-driven reconstitution of LGR5$^+$ ISCs, we sought to distinguish whether this effect was mediated by bacterial components or relative microbial metabolites. To this end, we administered BC culture supernatant (BC.sup) or heat-inactivated (HI) BC to DSS-treated mice (Supplementary Fig. 3a–i). BC.sup significantly alleviated disease severity, whereas HI BC was ineffective (Fig. 4a–c, and Supplementary Fig. 3b–e). This indicates that BC-derived metabolites, rather than structural components, are responsible for the protection, likely by facilitating the regeneration of LGR5$^+$ aISCs from HOPX$^+$ rISCs.

To test this, we conducted a quasi-targeted metabolomic analysis on cIECs isolated from BC-colonized and Veh-treated mice at D3 post-DSS challenge. KEGG pathway enrichment analysis revealed significant downregulation of ketone body metabolism (butanoate pathway) in Veh-treated controls compared to BC-colonized mice (Fig. 4d). Consistent with this, BC colonization markedly elevated β-hydroxybutyrate (BHB) levels within cIECs at this time point (Fig. 4e).

We next assessed the kinetics of BHB production in cIECs from BC-colonized and control mice. BC colonization resulted in significantly increased BHB levels at D0, D1, and D3 post-DSS induction, although a gradual decrease was observed over time within the BC group (Fig. 4f, and Supplementary Fig. 3a-ii).

To determine whether BHB is directly produced by BC, we performed whole-genome screening and found that BC lacks key genes for BHB biosynthesis (Fig. 4g). Consistent with this, BHB levels in BC culture supernatant (BC.sup) were comparable to those in the chopped meat carbohydrate (CMC) medium control after 48 h of culture (Fig. 4h). These results indicate that BC does not secrete BHB, but instead may enhance ketone body metabolism within cIECs, leading to increased local BHB production.

We next investigate whether BHB promotes intestinal epithelium regeneration through HOPX$^+$ rISCs. To this end, we generated a TAM-inducible HOPX conditional knockout mouse model by crossing *Bmi1-Cre^{ERT2}* mice with *Hopx$^{fl/fl}$* mice (*Bmi1^{CreERT2}Hopx$^{fl/fl}$*, termed as *Hopx$^{\Delta rISC}$*)

https://doi.org/10.1038/s41467-026-70062-6

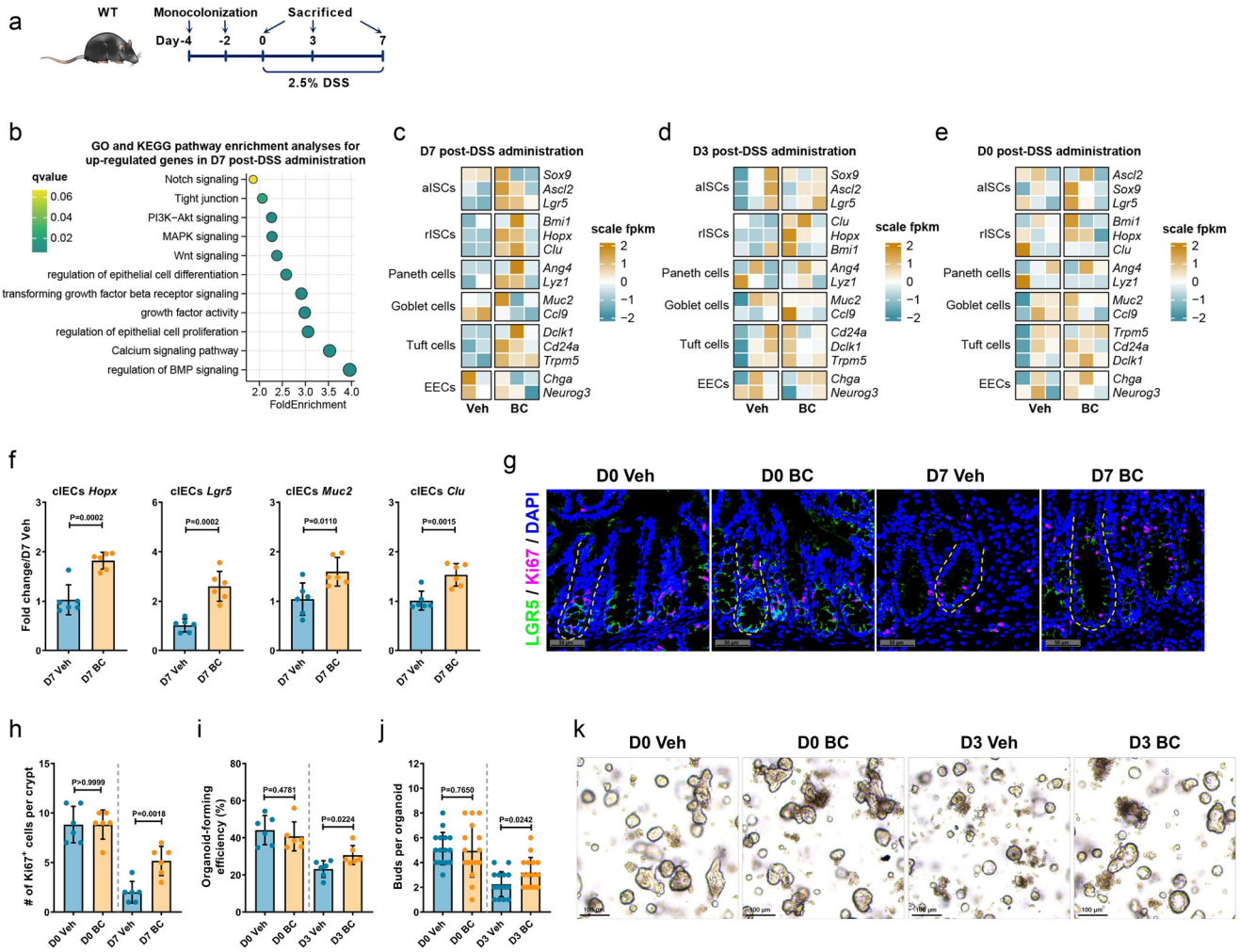

Fig. 2 | *B. coccoides* colonization rescues the loss of LGR5⁺ ISCs and promotes epithelial regeneration. a Experimental schematics of DSS treatment in BC-colonized WT mice. **b** GO and KEGG pathway enrichment analyses of upregulated genes in colonic intestinal epithelial cells (cIECs) from DSS-treated C57BL/6J mice colonized BC ($n = 3$) vs. vehicle (Veh, $n = 2$) at D7. Functional enrichment significance was assessed using the clusterProfiler package, with false discovery rate controlled by q values estimated using the Storey method. **c**–**e** Heatmaps of cell-specific marker expression in cIECs. **f** qRT-PCR of *Hopx*, *Lgr5*, *Muc2* and *Clu* in cIECs ($n = 6$) at D7 post-DSS. **g** Ki67/LGR5 immunofluorescence in colon tissues from BC/Veh-colonized mice with or without DSS. **h** Ki67⁺ cells/crypt (IFA, $n = 6$). **j**, **k** Primary crypt cultures and crypt count at D0/D3 post-DSS: (**i**) Organoid-forming efficiency ($n = 6$); (**j**) Number of buds per organoid ($n = 15$); (**k**) Representative images. Data represent mean ± SD from ≥2 independent experiments. Statistical significance determined by two-sided Student's t-test. Source data are provided as a Source Data file.

to enable specific deletion of *Hopx* in *Bmi1*-expressing rISCs (Supplementary Fig. 3a-iii). Although BHB levels in cIECs were significantly increased in $Hopx^{\Delta rISC}$ mice prior to DSS challenge (Fig. 4i), TAM-induced *Hopx* deletion abrogated the enhancing effects of BHB on crypt regeneration. In contrast to $Hopx^{fl/fl}$ littermate controls, which showed increased in LGR5⁺ and Ki-67⁺ cells per crypt following BHB treatment at D7 post-DSS, $Hopx^{\Delta rISC}$ mice exhibited markedly diminished regenerative responses (Fig. 4j–l). Consistently, loss of *Hopx* in the rISCs reversed the beneficial effects of BHB on disease phenotypes, histopathology, IL-6⁺ macrophage infiltration, and expression of tight junctions, *Muc2*, and inflammatory cytokines (Fig. 4m–o, and Supplementary Fig. 3f). These results demonstrate that HOPX expression in rISCs is essential for BHB-mediated restoration of the LGR5⁺ active ISC pool, thereby driving epithelial regeneration and ameliorating colitis.

To evaluate the translational relevance of this mechanism, we examined whether BHB also facilitates the transition from HOPX⁺ rISCs to LGR5⁺ aISCs in human colonic organoids following inflammatory injury. Organoids pretreated with BHB were injured with TNFα/IFNγ (stimulation, ST), and expression of LGR5 and HOPX was assessed at 0, 6, and 24 h post treatment (hpt) (Supplementary Fig. 3a-iv). At baseline (0 hpt), BHB suppressed LGR5 and enhanced HOPX expression, suggesting a homeostatic inhibition of LGR5⁺ aISC proliferation. Following injury (6 hpt), ST alone downregulated LGR5 and upregulated HOPX, with further amplification of HOPX and p-STAT1, a key regulator of rISC activation during regeneration[25] in BHB-treated groups (Fig. 4p, q, and Supplementary Fig. 3g). By 24 hpt, however, BHB promoted a pronounced shift toward LGR5 expression with concurrent downregulation of HOPX (Fig. 4p, r), indicating accelerated regeneration through rISC-to-aISC differentiation. Thus, combining in vivo murine models and human ex vivo organoids, we identify that BHB (derived from BC colonization) drives epithelial regeneration through a conserved, HOPX-dependent core mechanism: the activation of HOPX⁺ rISCs to ultimately reconstitute the functional LGR5⁺ aISC compartment.

BC cooperates with IPA-producing commensals to activate HOPX⁺ rISCs

Our recent work established that the microbial tryptophan catabolite indole-3-propionic acid (IPA) activates peroxisome proliferator-activated receptor alpha (PPARα), thereby stimulating 3-hydroxy-3-methylglutaryl-CoA synthetase 2 (HMGCS2)-mediated ketogenesis and

https://doi.org/10.1038/s41467-026-70062-6

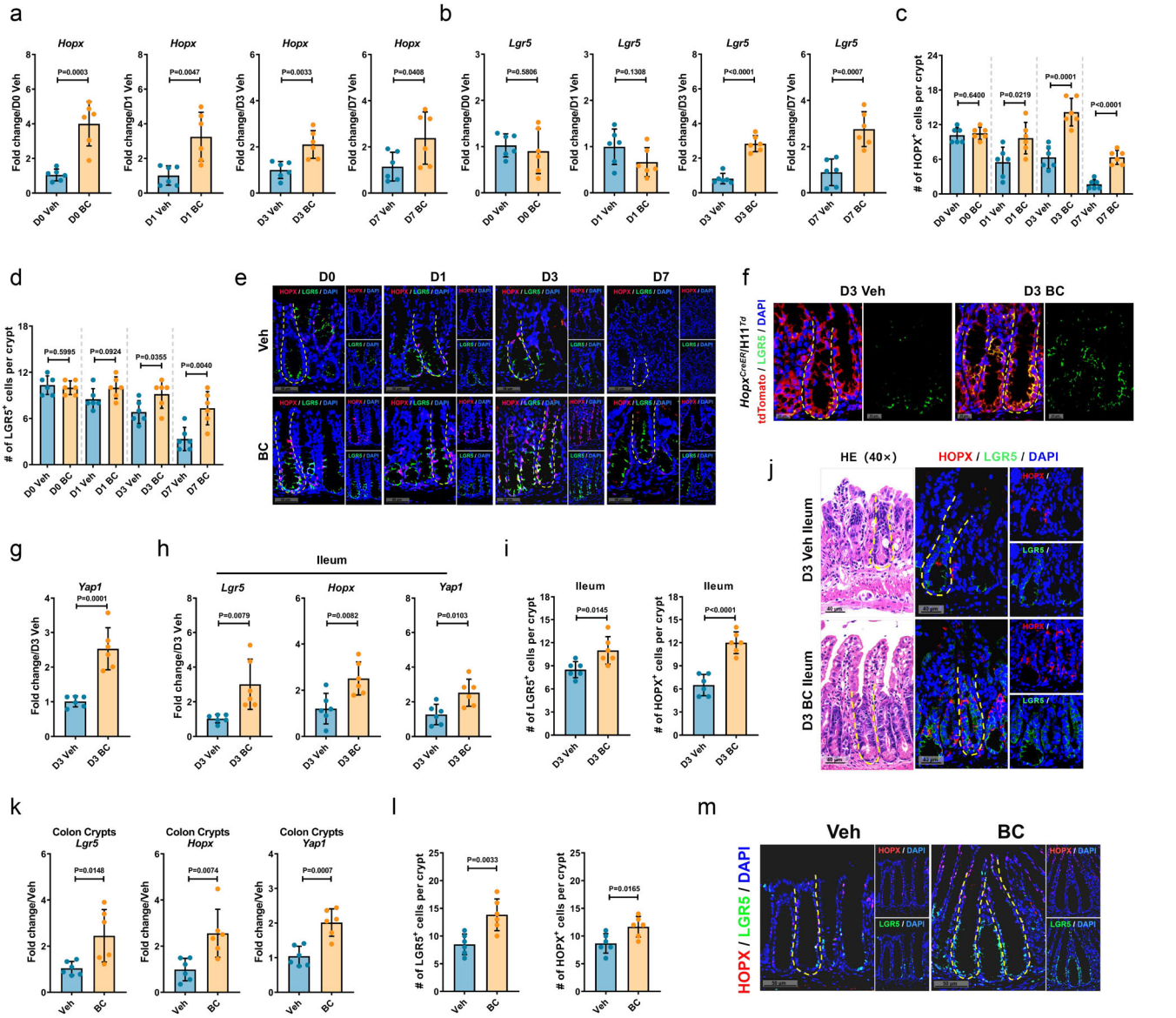

Fig. 3 | *B. coccoides* induces HOPX⁺ rISCs to reconstitute depleted LGR5⁺ ISCs following acute mucosal injury. Temporal *Hopx* (**a**) and *Lgr5* (**b**) expression in colonic crypts of WT mice treated with BC post-DSS ($n = 6$). **c**–**e** Quantification of HOPX⁺ and LGR5⁺ cells/crypt (IFA) in DSS model ($n = 6$). **f** Lineage tracing in *Hopx*^{CreER}/H11^{Td} mice co-staining for LGR5. **g** *Yap1* expression in DSS model ($n = 6$). RE model analysis (16 Gy IR, $n = 6$, biologically independent samples): (**h**) *Lgr5, Hopx* and *Yap1* (qRT-PCR); (**i**, **j**) LGR5 and HOPX (IFA). Therapeutic BC post-DSS (n = 6): (**k**) *Lgr5*, *Hopx* and *Yap1* expression (qRT-PCR); (**l**, **m**) LGR5 and HOPX (IFA). Data represent mean ± SD from ≥2 independent experiments. Statistical significance determined by two-sided Student's *t*-test. Source data are provided as a Source Data file.

BHB production, a metabolic cascade essential for the expansion of the LGR5⁺ ISC pool and subsequent mucosal regeneration[26]. We therefore hypothesized that BC may enhance BHB production via IPA synthesis, ultimately activating HOPX⁺ rISCs to replenish LGR5⁺ aISCs lost during mucosal injury.

To test this hypothesis, we measured IPA levels in colon tissues before DSS challenge (D0) using UHPLC-MS/MS. The results showed that BC-colonized mice had significantly higher IPA concentrations than Veh-treated controls (Fig. 5a, and Supplementary Fig. 4a–i). Surprisingly, subsequent analysis of BC.sup cultured for 48 h in CMC medium revealed no elevated IPA or indole-3-acrylic acid (IA) production. Instead, we detected high concentrations of indole-3-lactic acid (ILA), another Trp-derived metabolite that lies upstream of IA and IPA in the microbial catabolic pathway[27] (Fig. 5b), suggesting that BC could only catabolize Trp into ILA and not further into IA or IPA.

We next evaluated whether ILA or IPA could promote the transition from HOPX⁺ rISCs to LGR5⁺ ISCs in a manner comparable to BHB using in vitro organoid models. Human colonic organoids pretreated with ILA or IPA were subjected to TNFα/IFNγ-induced injury. Both IPA and BHB significantly increased HOPX expression while suppressing LGR5 at 0 and 6 hpt (Figs. 4p, 5c, d, and Supplementary Fig. 4b). They conversely induced LGR5 upregulation alongside HOPX downregulation by 24 and 48 hpt (Fig. 5d, e, and Supplementary Fig. 4c). In contrast, ILA elicited none of these responses: it neither enhanced HOPX nor reduced LGR5 expression at 0 or 6 hpt, nor did it reverse this expression pattern at the later time point (Fig. 5c, d, and Supplementary Fig. 4b). Similarly, in colonic organoids derived from GF mice, ILA failed to early induce *Hopx* upregulation or *Lgr5* downregulation, and did not exhibit the late-phase transition to elevated *Lgr5* with concomitant *Hopx* reduction, as observed with both IPA and BHB (Fig. 5f, and Supplementary Fig. 4a-iii, -iv).

https://doi.org/10.1038/s41467-026-70062-6

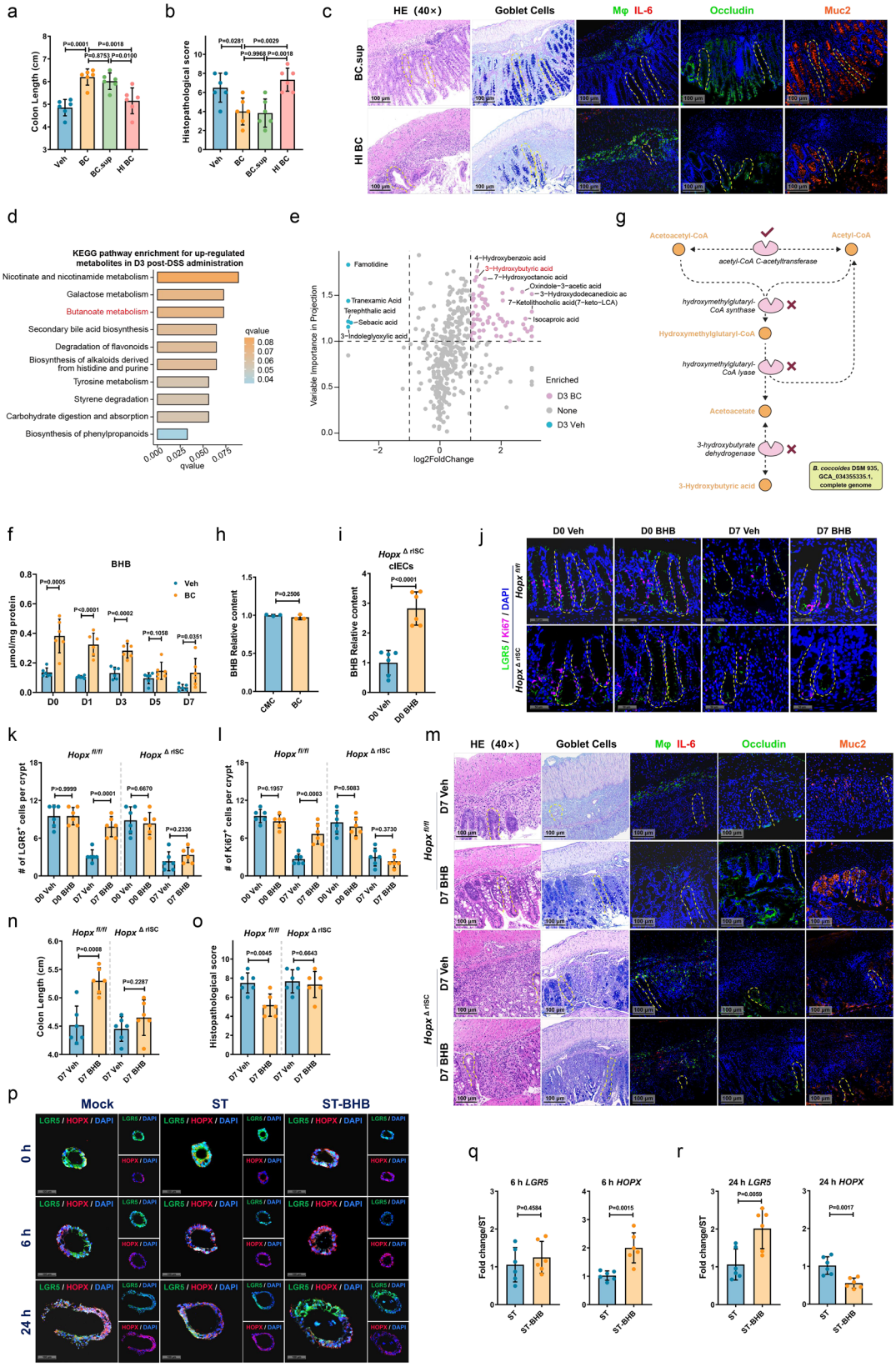

To further validate that ILA itself cannot activate HOPX⁺ rISCs to restore LGR5⁺ aISCs following injury without microbial conversion to IPA, in vivo we administered ILA or IPA to GF mice (Supplementary Fig. 4a-v). As anticipated, ILA treatment in GF mice failed to upregulate the expression of *Lgr5*, *Hopx*, or *Yap1*, and did not increase the number of LGR5⁺ or HOPX⁺ cells in colonic crypts at D3 post-DSS administration, in contrast to the effects observed with IPA treatment (Fig. 5g–j). Consistent with these findings, GF mice receiving ILA showed no increase in colonic IPA or BHB levels (Supplementary Fig. 4e, f). These results support the hypothesis that BC depends on cooperative interactions with other commensal microbes for IPA production.

Fig. 4 | *B. coccoides* and BHB compensate for LGR5⁺ ISC depletion to restore intestinal epithelium regeneration through HOPX. a–c Phenotypes of BC. sup/HI BC in WT mice with DSS administration ($n = 6$). **d** Bar plot shows the KEGG pathway enrichment results of upregulated metabolites at D3. Functional enrichment significance was assessed using the clusterProfiler package, with false discovery rate controlled by q values estimated using the Storey method. **e** Volcano plot shows the differentially abundant metabolites between the Veh ($n = 4$) and BC ($n = 4$) group at D3. **f** Temporal β-hydroxybutyrate (BHB) levels in cIECs post-DSS ($n = 6$). **g** Schematic of the process of BHB production, highlighting the absence of enzymes in the BC genome that are essential for BHB production. **h** BHB concentration was determined in BC and chopped meat carbohydrate medium (CMC) after 48 h culture ($n = 3$, biologically independent samples). *Hopx*$^{fl/fl}$ and *Hopx*$^{\Delta rISC}$ mice treated with BHB post-DSS ($n = 6$): BHB levels in cIECs (**i**), Ki67/LGR5 IFA (**j–l**), colon length (**n**), histopathology (**m**, **o**), and mucin/goblet markers (**o**). **p–r**, HOPX/LGR5 dynamics in human organoids post-cytokine injury with or without BHB pretreatment ($n = 6$). Data represent mean ± SD from ≥2 independent experiments. Statistical significance determined by two-sided Student's t-test or one-way ANOVA followed by Tukey's post hoc test for multiple comparisons. Source data are provided as a Source Data file.

Given the established role of *P. russellii* and *C. sporogenes* in converting ILA to IPA, we first analyzed public metagenomic data from IBD cohorts and found a significant positive correlation between the abundance of BC and these IPA-producing bacteria (Fig. 5k, and Supplementary Fig. 4g). We therefore selected them as representative commensals to test our hypothesis of functional synergy.

In vitro, when BC was co-cultured with either *P. russellii* or *C. sporogenes*, both partners exhibited a synergistic increase in absolute abundance compared to monocultures, indicating mutual growth promotion (Fig. 5l). Consistent with this, UHPLC-MS/MS analysis showed that co-culture with BC significantly enhanced IPA production by these strains (Fig. 5m).

We next examined this interaction in vivo. In conventional WT B6 mice, BC gavage increased fecal levels of *P. russellii* and *C. sporogenes* (Fig. 5n, and Supplementary Fig. 4a-i), accompanied by elevated concentrations of both ILA and IPA (Fig. 5o, p, and Supplementary Fig. 4h), supporting the presence of a metabolically synergistic relationship.

To further determine whether this synergy functionally impacts IPA production and HOPX⁺ rISC induction, we turned to a GF mouse model. Compared to monocolonization with BC, co-colonization with BC plus *P. russellii*. or *C. sporogenes* further enhanced the expression of *Lgr5*, *Hopx*, and *Yap1* (Fig. 5q, and Supplementary Fig. 4i-i, -ii, -iii). Metabolite analysis confirmed that BC alone produced ILA but not IPA, whereas *P. russellii*/*C. sporogenes*, with BC, significantly increased fecal IPA (Fig. 5r, s). These results demonstrate that BC-derived ILA requires further metabolism to IPA by specific commensals such as *P. russellii* or *C. sporogenes* to fully activate the HOPX⁺ rISC program.

BC phenyllactate dehydrogenase activity produces ILA and improves IPA-mediated LGR5⁺ ISC reconstitution via HOPX

We next investigated the metabolic pathway underlying ILA production in BC. Comparative genomic analysis revealed that BC encodes a homolog of phenyllactate dehydrogenase (*fldH*), which shares 40.36% amino acid identity with the established fldH enzyme in *C. sporogenes*, a key catalyst in the conversion of Indole-3-pyruvate (IPYA) to ILA (Fig. 6a). Structural modeling further supported functional conservation between the BC and *C. sporogenes* fldH proteins (Fig. 6b).

Although direct knockout of *fldH* in BC would be the most rigorous approach to validate its role in ILA biosynthesis and host protection, genetic manipulation in this strain remains technically challenging. As an alternative, we heterologously expressed the BC-derived *fldH* gene in *Escherichia coli* (generating *E. coli-fldH*) to directly evaluate its enzymatic function. When cultured in brain heart infusion (BHI) medium supplemented with varying concentrations of tryptophan (Trp), *E. coli-fldH* produced significantly higher levels of ILA and concomitantly reduced Trp concentrations compared to the empty vector control strain (*E. coli-VEC*) (Fig. 6c, d). Notably, even in the absence of Trp supplementation, *E. coli-fldH* generated ILA at levels comparable to those produced by BC (Fig. 6c, e). These results confirm that fldH enzyme actively drives ILA synthesis through Trp degradation and confers this metabolic capability to heterologous hosts.

To determine whether BC-derived fldH enzyme promotes ILA biosynthesis to drive IPA production and facilitate LGR5⁺ ISC regeneration during epithelial injury, we colonized conventional WT B6 mice with either *E. coli-VEC* or *E. coli-fldH* and subjected them to DSS-induced colitis (Fig. 6f). Mice monocolonized with *E. coli-fldH* exhibited significantly elevated IPA levels in colon relative to *E. coli-VEC* controls (Fig. 6g). By D3 post-DSS challenge, *E. coli-fldH*-colonized mice further demonstrated marked upregulation of *Hopx*, *Lgr5*, and *Yap1*, both transcriptionally and translationally in colonic crypts (Fig. 6h, i), accompanied by increased BHB concentrations within cIECs (Fig. 6j). By D7 post-DSS administration, these mice also displayed expanded LGR5⁺ and Ki-67⁺ cell populations per crypt (Fig. 6k–m), attenuated disease phenotypes and histopathological damage, elevated expression of tight junction proteins and *Muc2*, and reduced *Tnfa* levels compared with controls (Fig. 6n–q).

Finally, we evaluated whether a tryptophan-depleted diet (TDD), which markedly reduces microbially derived indole metabolites[28], compromises HOPX⁺ rISC activation and LGR5⁺ aISC renewal during mucosal injury (Fig. 7a). TDD significantly diminished IPA levels within cIECs (Fig. 7b) and exacerbated DSS-induced colonic shortening and histopathological injury. These deficits were effectively rescued by either IPA supplementation or concurrent Trp reintroduction together with *E. coli-fldH* colonization (Fig. 7c–e). Consistent with these phenotypic observations, TDD-mediated downregulation of *Hopx*, *Lgr5*, and *Yap1*, in colonic crypts was reversed upon IPA administration or combined Trp-*E. coli-fldH* treatment (Fig. 7f, g). Together, these findings support a model in which BC-produced ILA serves as a metabolic precursor for IPA, which in turn activates HOPX⁺ rISCs and promotes LGR5⁺ ISC-mediated epithelial regeneration, ultimately accelerating mucosal repair and disease remission.

Discussion

Dysregulation of ISCs impairs epithelial barrier integrity and contributes significantly to the pathogenesis of intestinal disorders. Growing evidence underscores the importance of gut microbiota and their metabolic derivatives in promoting epithelial regeneration following intestinal injury. Nevertheless, the specific microbial metabolites involved and their mechanisms of action in ISC-mediated repair remain poorly defined. In this study, we identify BC as a key commensal bacterium that facilitates intestinal epithelial regeneration by activating HOPX⁺ rISCs to restore the LGR5⁺ ISC compartment, a process potentiated through metabolic cooperation with IPA-producing bacteria (Fig. 7h). Our findings advance the limited understanding of conserved bacterium-host metabolic crosstalk that is essential for epithelial homeostasis and repair, with relevance to IBD, RE, and potentially other conditions involving epithelial damage.

IBD is associated with profound microbial dysbiosis, characterized by altered community structure and metabolic output. Metagenomic analyses of public datasets reveal a consistent depletion of BC in IBD cohorts across diverse geographic regions (Fig. 1d–g). Although establishing direct clinical correlations between BC abundance and disease progression remains challenging (due in part to limited longitudinal sample availability), our controlled studies in DSS-induced colitis models demonstrate an unequivocal protective role for BC. Monocolonization of conventional mice with BC significantly attenuated colitis severity and enhanced mucosal barrier function (Fig. 1i–l). These results are corroborated by earlier work from

https://doi.org/10.1038/s41467-026-70062-6

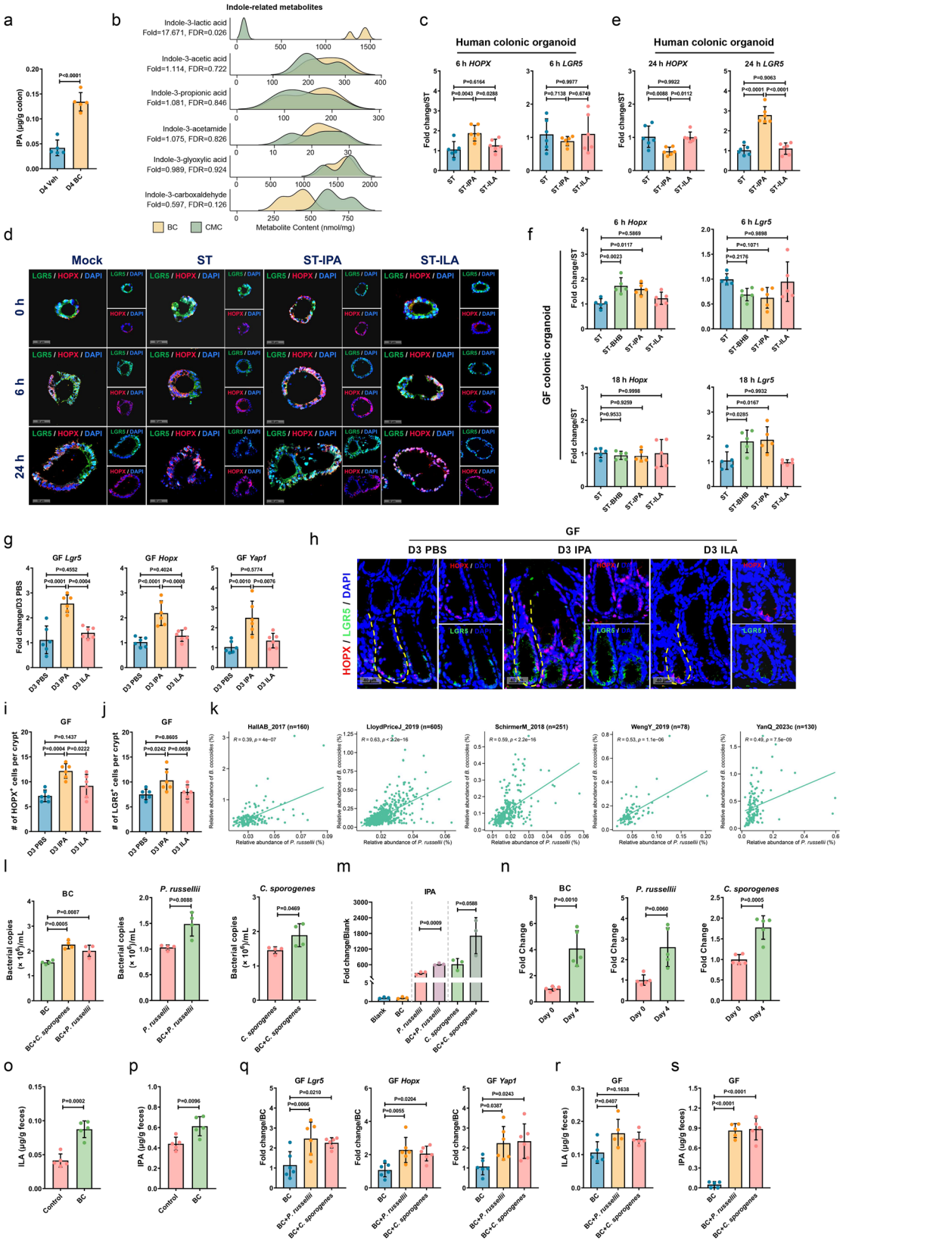

Holmberg et al., which reported that BC supplementation promotes colonic mucus layer expansion via short-chain fatty acid production[29], further supporting its role in mucosal protection.

Through the integration of RNA-seq, lineage tracing, and conditional ablation approaches, our study reveals a regulatory mechanism by which BC enhances BHB production in IECs, leading to the activation of a rISC population marked by HOPX expression (Figs. 3 and 4). Once activated, these HOPX$^+$ rISCs demonstrate the capacity to regenerate a LGR5$^+$ ISC pool and play a critical role in epithelial repair in both DSS-induced colitis and RE models (Fig. 3). While our data indicate that IEC-derived BHB promotes HOPX$^+$ rISC activation, the precise epithelial

Fig. 5 | *B. coccoides* cooperates with IPA-producing commensals to activate HOPX⁺ rISCs. a Colonic IPA in WT mice colonized with BC ($n = 5$). **b** Ridge plots visualize the distribution of indole-related metabolite concentrations in BC supernatant ($n = 3$) and control (chopped meat carbohydrate medium, CMC) samples ($n = 3$). The statistical significance was estimated using two-sided Welch *t*-test, followed by BH correction for multiple comparisons. HOPX and LGR5 dynamics in human organoids (**c**–**e**, $n = 6$) and GF colonic organoids (**f**, $n = 5$) post-cytokine injury with or without IPA/ILA pretreatment. Colonic HOPX/LGR5 expression in GF mice (**g**: qRT-PCR; **h**–**j**: IFA; $n = 6$). **k** Scatter plots illustrate the correlation between the metagenomic relative abundances of BC and *P. russellii* across five publicly available IBD cohorts. Spearman's rank correlation was used to calculate the correlation coefficient and corresponding statistical significance. **l** Absolute abundance of BC, *P. russellii* and *C. sporogenes* in monoculture versus co-culture systems ($n = 4$). **m** UHPLC-MS/MS analysis of IPA production by *P. russellii* or *C. sporogenes* in co-culture with BC ($n = 3$). **n** Fecal levels of BC, *P. russellii* and *C. sporogenes* in WT mice following BC gavage ($n = 5$). **o**, **p** Fecal concentrations of ILA and IPA in WT mice with or without BC gavage ($n = 5$). GF mice following mono- or co-colonization with the indicated bacterial strains: Expression of *Lgr5*, *Hopx* and *Yap1* in cIECs at D3 post-DSS (**q**, $n = 6$), fecal concentrations of ILA and IPA at D0 post-DSS (**r**, **s** $n = 5$). Data represent mean ± SD from ≥2 independent experiments. Statistical significance determined by two-sided Student's *t*-test or one-way ANOVA followed by Tukey's post hoc test for multiple comparisons. Source data are provided as a Source Data file.

subpopulation responsible for BHB generation in our injury model remains to be determined. Previous work in homeostatic conditions identified LGR5⁺ CBCs as a major source of BHB, which maintains stemness via HDAC inhibition and Notch signaling[30]. In our DSS-injury setting, however, LGR5⁺ cells are rapidly depleted, making it technically difficult to isolate them for source tracing. Future studies using single-cell metabolomics or in situ activity reporters may help resolve this spatial question. Moreover, the molecular mechanism linking BHB to HOPX induction warrants deeper investigation. Recent studies show that BHB can induce histone H3K9 beta-hydroxybutyrylation (H3K9bhb), an epigenetic mark associated with activation of metabolic and differentiation genes[31]. Whether BHB regulates HOPX through similar chromatin remodeling represents a compelling direction for future work.

Our results are consistent with previous work identifying a HOPX⁺-dependent regenerative cell population that contributes substantially to mucosal healing[12]. Specifically, we observed that BC treatment in HOPX lineage-tracer mice led to an increase in HOPX⁺ daughter cells co-expressing LGR5 within crypts at D3 post-DSS challenge (Fig. 3f), supporting the plasticity of HOPX⁺ cells in replenishing the injury-depleted LGR5⁺ ISC compartment. It is worth noting that another rISC subset marked by high *Clu* expression has also been shown to restore the LGR5⁺ pool after injury[14]. It reported that low HOPX expression in CLU^{high} rISCs, which may appear discrepant with our findings. However, the injury model (radiation vs. chemical DSS), timing of analysis, and regenerative niches examined differ substantially, likely explaining these phenotypic variations. Together, these observations highlight the context-dependent plasticity and heterogeneity of rISC populations during repair.

Current therapies for IBD primarily target immune suppression often through inhibition of cytokines such as TNFα[32,33], which carries risks of infections and neoplastic events[33,34]. These limitations underscore the need for treatment strategies that promote mucosal healing without broad immunosuppression. Here, we demonstrate that a commensal BC strain expressing *fldH* generates ILA from Trp catabolism, and synergizes with *P. russellii* or *C. sporogenes* to produce IPA both in vitro and in vivo (Figs. 5l–p and 6c–g). Our work adds to growing evidence that microbial co-metabolism and cross-feeding critically shape host-active metabolite output. A recent study showed that in a defined community, fiber-derived sugars provided by *Bacteroides thetaiotaomicron* suppressed indole production in *E. coli* via catabolite repression, thereby increasing Trp availability for *C. sporogenes* to produce ILA and IPA[35]. Similarly, BC may create a metabolic niche that facilitates the growth or activity of IPA-producing partners, possibly through provision of carbon sources or acidification[36], which we will explore in future work. The broader relevance of such metabolic partnerships is further highlighted by a recent report that *Lactobacillus johnsonii* cooperates with *C. sporogenes* to produce IPA, which enhances anti-tumor CD8⁺ T cell stemness and improves immune checkpoint blockade efficacy across cancer types[37]. This underscores the potential translatability of targeting microbial metabolic networks for therapeutic benefit.

Our study has several limitations. First, although we demonstrate that BC encodes a functional *fldH* gene and that expressing BC *fldH* in *E. coli* confers ILA production, genetic manipulation in BC remains technically challenging. Thus, we could not generate a BC-Δ*fldH* mutant to formally prove the requirement of this gene in the native bacterium. Developing robust genetic tools for BC will be essential for definitive functional studies. Second, while we used both male and female mice in our main colonization experiments and observed no significant sex-based differences in BC's protective effects, we acknowledge that DSS colitis severity[38] and IBD pathogenesis[39] are known to differ between sexes. Future studies should systematically evaluate potential sex differences in BC colonization dynamics, metabolite production and stem cell responses. Finally, although our multi-omics and functional data support a role for BC-driven BHB in activating HOPX⁺ rISCs, the downstream epigenetic or transcriptional mechanisms linking BHB to HOPX induction are yet to be fully elucidated.

In conclusion, our work identifies BC as a commensal bacterium that promotes intestinal epithelial regeneration through a BHB-HOPX⁺ rISC axis, amplified by metabolic interaction with IPA-producing bacteria. These findings highlight the therapeutic potential of targeting conserved microbial metabolic networks to stimulate endogenous repair mechanisms in IBD and other epithelial injury conditions.

Methods

Microbe strains

All microbe strains were described in the Supplementary Table 1. *P. russellii* was cultured in chopped meat carbohydrate broth (TOPBIO) medium (Hopebio) at 37 °C for 48 h under an atmosphere of 10% CO_2, 10% H_2 and 80% N_2 in an anaerobic incubator (AW300SG, Pummiero Scientific). *C. sporogenes* and *B. coccoides* (BC) were grown in MRS medium (LAND BRIDGE) or chopped meat carbohydrate broth (CMC) medium (Hopebio) respectively at 37 °C under the same anaerobic conditions (10% CO_2, 10% H_2, 80% N_2) for 48 h. *E. faecalis* (EF) was cultured in Lysogeny broth medium (Oxoid) at 37 °C for 48 h under aerobic conditions.

For metabolite supplementation studies, culture media were supplemented with varying concentrations of L-tryptophan (Trp) as specified in the respective figures, followed by sterilization via autoclaving. All bacterial strains were cultured in biological triplicate under aerobic conditions. Uninoculated media served as negative controls. Following 24-h fermentation, optical density at 600 nm (OD_{600}) was quantified using a spectrophotometer (BioTek Synergy H1), after which cultures were immediately chilled on ice. Cellular fractions were separated by centrifugation (16,000 × *g*, 10 min, 4 °C; Eppendorf 5424R), with 1 mL aliquots processed per sample.

Bacterial count

After 48 h of culture, the bacteria were collected and serially diluted tenfold on respective culture plates and CFUs were counted after 16 h incubation at 37 °C. Specifically, *P. russellii, C. sporogenes* and BC dilutions were cultured on Trypticase soy agar with defibrinated sheep

https://doi.org/10.1038/s41467-026-70062-6

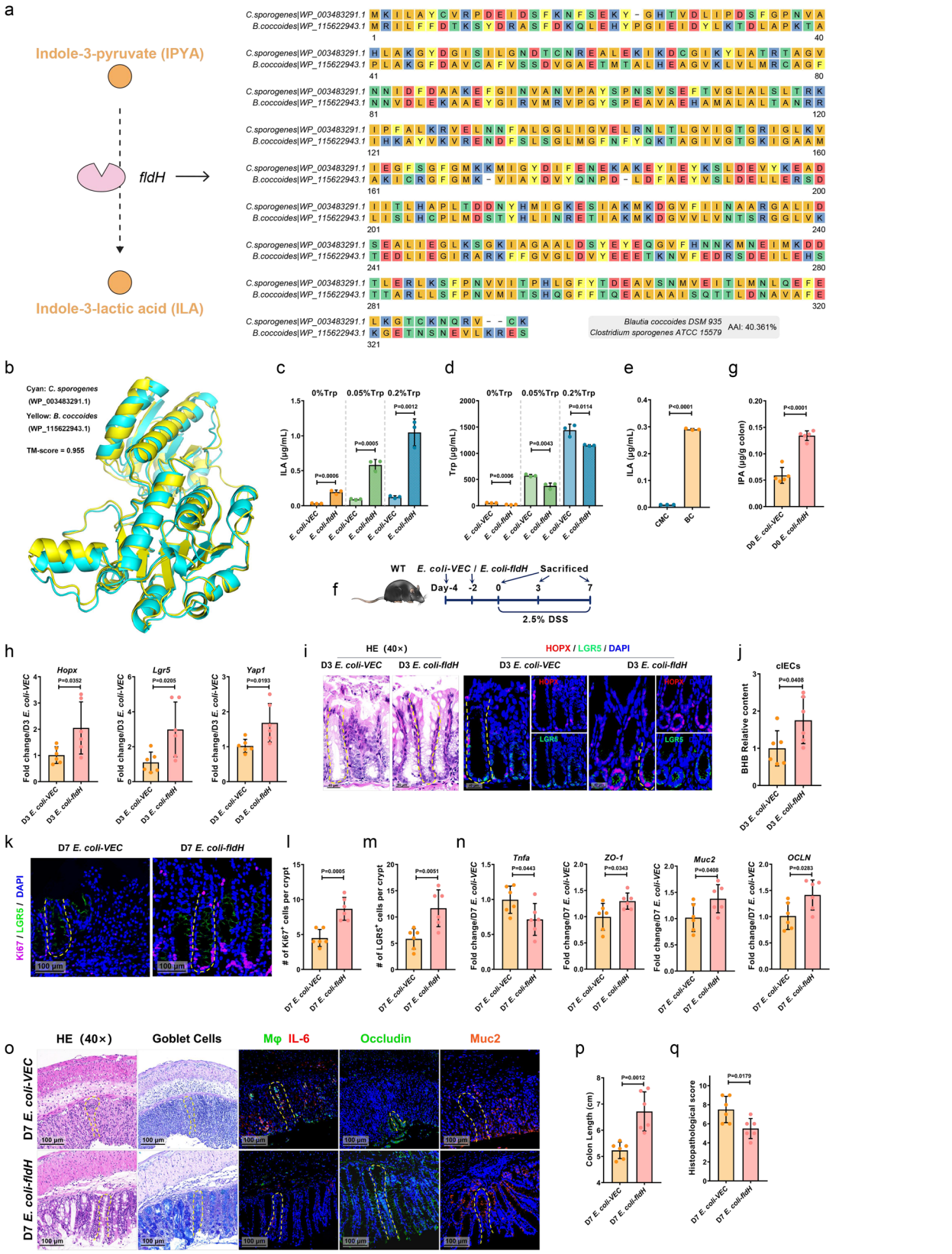

blood under anaerobic conditions in an anaerobic incubator (AW300SG, Pummiero Scientific). *E. faecalis* dilutions were cultured on Trypticase soy agar with defibrinated sheep blood. *E. coli-VEC* and *E. coli-fldH* dilutions were cultured on LB agar under aerobic conditions in an incubator (LRH-500F, Shanghai Bluepard Instruments CO., LTD). The bacterial cells were then pelleted by centrifugation at 6000 × *g* at 4 °C for 10 min, washed, and re-suspended in sterile reduced PBS buffer to achieve a specific density suitable for mouse gavage. These operations were conducted under anaerobic conditions in an anaerobic incubator (AW300SG, Pummiero Scientific) (*P. russellii, C. sporogenes* and BC) or under aerobic conditions (*E. faecalis, E. coli-VEC* and *E. coli-fldH*).

Fig. 6 | *B. coccoides* phenyllactate dehydrogenase activity produces ILA and improves IPA-mediated LGR5⁺ ISC reconstitution via HOPX. a Amino acid sequence alignment of the *fldH* enzyme involved in tryptophan (Trp) metabolism between BC and *C. sporogenes*. **b** Structural comparison of the *fldH* enzyme between BC (Yellow) and *C. sporogenes* (Cyan). **c**, **d** ILA and Trp concentrations in Trp-supplemented BHI medium by *E. coli* strains carrying empty vector (VEC) or the *fldH* gene ($n = 3$). **e** ILA concentration was determined in BC and chopped meat carbohydrate medium (CMC) after 48 h culture ($n = 3$, biologically independent samples). **f**–**q** WT-DSS model colonized with *E. coli-VEC/E. coli-fldH*: D0 colonic IPA concentrations (**g**, $n = 5$); D3 ISC markers (**h**, **i**, $n = 6$); D3 BHB concentrations in cIECs (**j**, $n = 6$); Ki67 and LGR5 (IFA) in colon at D7 post-DSS (**k**–**m**, $n = 6$); qRT-PCR of *Tnfa* in colon and *OCLN*, *ZO-1*, *Muc2* in cIECs (**n**, $n = 6$); D7 phenotypes (**o**–**q**, $n = 6$). Data represent mean ± SD from ≥2 independent experiments. Statistical significance determined by two-sided Student's *t*-test. Source data are provided as a Source Data file.

Human participants

Fecal samples were collected from 28 healthy controls (with no psychological or cognitive impairments) and from 32 patients with Crohn's disease (CD) at Sir Run Run Shaw Hospital, School of Medicine, Zhejiang University (Supplementary Table 1). All patients were diagnosed according to European Crohn's and Colitis Organization (ECCO) guidelines, including radiologic, endoscopic, clinical symptoms, and pathology. The patients were without antibiotics and probiotics in the month prior to sample collection. Other exclusion criteria included: history of bowel resection; pregnant or lactating women; age <18, or age >73. The sex information and baseline characteristics of the participants are shown in Supplementary Data 1. Stool samples were collected right after defecation and snap frozen for 16S rRNA sequencing. Informed consent was obtained from all participants, and the experimental protocol was approved by the Clinical Research Ethics Committee of the Clinical Research Ethics Committee of Sir Run Run Shaw Hospital, Zhejiang University School of Medicine (20210622-31). Participants did not receive financial compensation.

Human colonic tissues were collected at the First Affiliated Hospital of Guangdong Pharmaceutical University. Three individuals underwent colonoscopy as part of their routine health examinations, necessitating tissue removal for pathological biopsy due to the presence of intestinal polyps. Fresh normal mucosal tissues for human organoid culture were obtained from healthy regions of the intestinal tissue adjacent to the polyps, as identified and assessed by the physician during the tissue acquisition process. Informed consent was obtained from all participants, and the experimental protocol was approved by the Clinical Research Ethics Committee of the First Affiliated Hospital of Guangdong Pharmaceutical University (V1.0, 20210221). Participants did not receive financial compensation. The primary tissue samples were fully utilized in the process of organoid derivation and experimental analysis and are therefore not available for distribution. Requests concerning the study should be directed to the corresponding author.

Animals

All experiments used mice were described in the Supplementary Table 1. Germ-free (GF) C57BL/6J mice were bred and housed at the Shenzhen Gnotobio Biotechnology Co., Ltd. GF status was confirmed through 16S qPCR analysis before use in relevant experiments, which were also carried out at Shenzhen Gnotobio Biotechnology Co., Ltd. Wild-type C57BL/6J (WT) mice were purchased from the Model Animal Research Center of Nanjing University (Nanjing, China). *Hopx-CreERT2* mice were kindly provided by Dr. Bin Zhou from Institute of Biochemistry and Cell Biology, Shanghai Institutes for Biological Sciences, Chinese Academy of Sciences. *Hopx*-flox mice, *Bmi1-P2A-CreERT2* mice and *H11-CAG-LSL-tdTomato* mice were purchased from GemPharmatech Co., Ltd (Nanjing, China).

Unless otherwise stated, all experiments utilized 6–8-week-old male or female mice. No significant sex-dependent differences were observed in the reported experiments. The mice were housed in a specific-pathogen-free facility at Zhejiang University, where they were maintained under controlled conditions of temperature (22 ± 2 °C) and humidity (50 ± 10%), with a constant 12-h light/dark cycle. They had free access to a regular chow diet (P1101F-25, Suzhou SHUANGSHI) and water throughout the study. The ethical guidelines of the Animal Experimentation Ethics Committee of Zhejiang University (No. 27248) and IACUC of Gnotobio (JTAW20240615-1) were followed.

Colitis models and treatments

Unless otherwise specified, WT or certain knockout mice were administered 2.5% dextran sulfate sodium (DSS, Yeasen, 60316ES76) in their drinking water for 7 days to establish the DSS-induced colitis mouse model.

To assess the impact of bacterial strains on DSS-induced colitis, conventional WT mice were gavaged with 200 µL of PBS containing 10^9 CFU of bacteria twice within a 48-h interval, followed by DSS treatment.

To evaluate the therapeutic potential of BC in experimental colitis without pretreatment, conventional WT mice were first treated with 2.5% DSS in drinking water for 5 days. Subsequently, they were gavaged with 200 µL of PBS containing 10^9 CFU of BC twice within a 48-h interval, followed by regular water administration.

For the pasteurization (HI) experiments, WT mice were orally gavaged with 10^9 CFU of BC inactivated by pasteurization at 70 °C for 30 min, diluted in 200 µL PBS, for 5 days. DSS administration followed on the 6th day. The bacterial supernatants were prepared by centrifuging cultured BC at 6000 × *g* for 10 min at 4 °C, then filtering through polyether-sulfone filters (0.22 µm; Merck Millipore) to remove residual bacterial cells. WT mice were gavaged with 200 µL of these bacterial supernatants for 5 days, followed by DSS administration on the 6th day.

To investigate the effects of BC-derived metabolites, WT and GF mice were gavaged with indole-3-lactic acid (ILA, 50 mg/kg, dissolved in 200 µL PBS), indole-3-proponic acid (IPA, 200 mg/kg, insoluble, suspend thoroughly before gavage, 200 µL PBS per mouse) daily for 5 days before DSS treatment.

For the β-hydroxybutyrate (BHB) protection study, mice were gavaged with BHB at 40 mg/25 g (dissolved in 100 µL PBS) 16 h before DSS treatment.

To examine whether reduced IPA production could influence colitis progression, we designed a special diet that differed only in the absence of tryptophan (Trp) from the control diet (detailed composition in Supplementary Data 2; Wuxi Fanbo Biotechnology). WT mice were provided free access to either a Trp-depleted diet (TDD, Wuxi Fanbo Biotechnology, FB-A10022) or the control diet (Wuxi Fanbo Biotechnology, FB-A10021B) for 17 days. After 9 days on the TDD, mice were gavaged with Trp at 1 g/kg (insoluble, suspend thoroughly before gavage, 200 µL PBS per mouse) following bacterial colonization or with IPA at 200 mg/kg daily for 5 days, followed by DSS treatment.

For the 2,4,6-trinitrobenzene sulfonic acid (TNBS) model, mice were shaved on the back just below the neck and painted with 1% TNBS (Meilunbio, MB5523) mixed in an acetone/olive oil solution for presensitization (150 µL per mouse). After 7 days of presensitization, mice were anesthetized and maintained with 1.5% to 2.0% isoflurane. Subsequently, 2.5% TNBS in 100 µL of 50% ethanol solution was administered into the colon via a catheter inserted ~3 cm into the anus.

Radiation enteritis (RE) model

WT mice were anesthetized by intraperitoneal injection of 50 mg/kg Zoletil®50 (virbac) and 5 mg/kg Xylazine Hydrochloride (D005, Jilin Huamu Animal Health Product Co., Ltd), then treated with total

https://doi.org/10.1038/s41467-026-70062-6

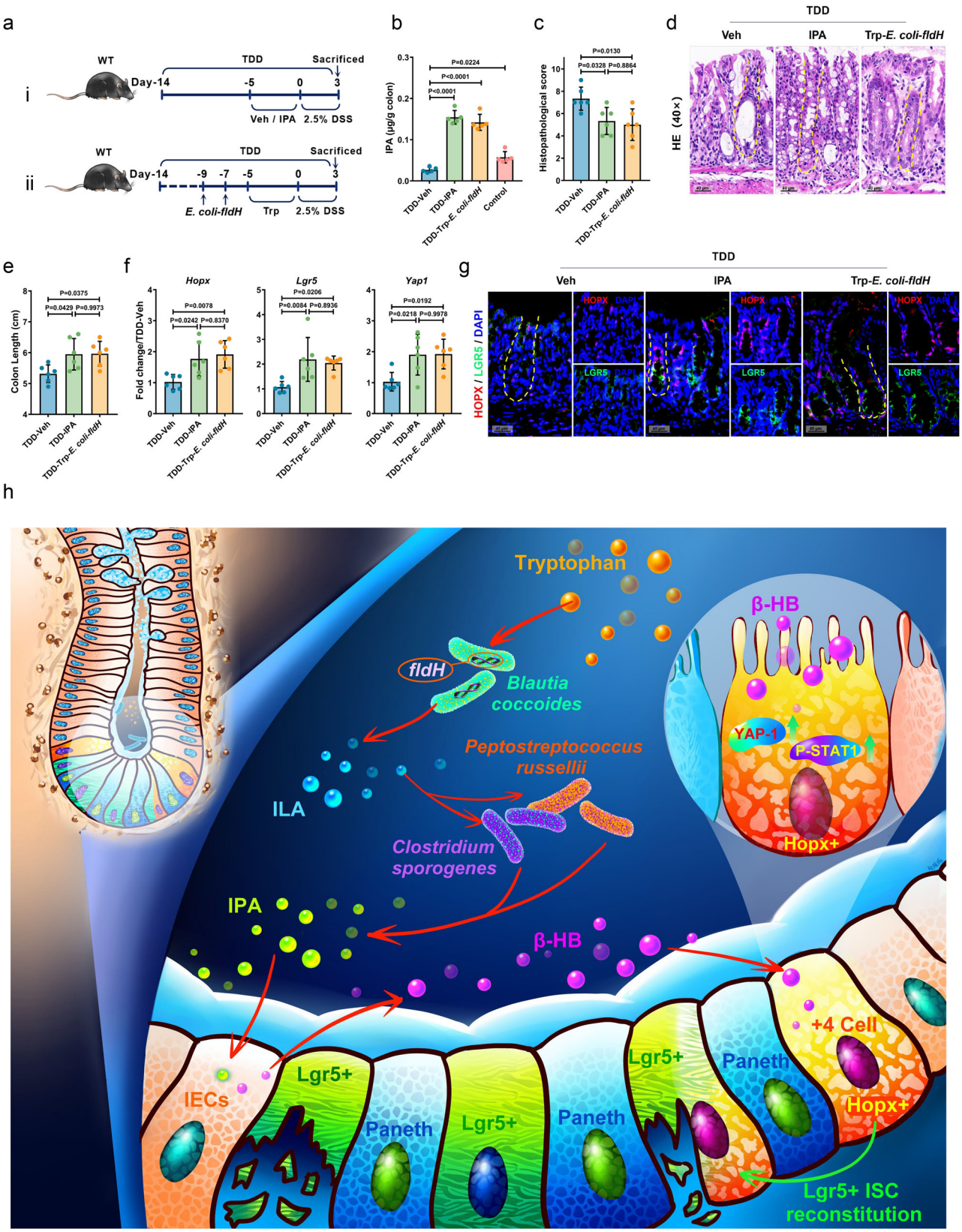

Fig. 7 | Dietary Tryptophan enhances IPA-mediated mucosal repair through *B. coccoides* phenyllactate dehydrogenase activity. a–**g** Experimental schematics: WT mice on Trp-depleted diet treated with IPA (200 mg/kg) or colonized with *E. coli-fldH* (10^9 CFU) + Trp (1 g/kg), then subjected to DSS administration (**a**). At D3 post-DSS, colonic IPA concentrations (**b**, n = 5), disease phenotypes (**c**–**e**, $n = 6$), mucosal repair markers (**f**, **g**, $n = 6$) were determined. **h** Mechanistic schema of microbiota-IPA-HOPX axis. Data represent mean ± SD from ≥2 independent experiments. Statistical significance determined by one-way ANOVA followed by Tukey's post hoc test for multiple comparisons. Source data are provided as a Source Data file.

abdominal irradiation with a single irradiation dose of 16 Gy (γ-ray) at a rate of 1.0 Gy/min in a Siemens Primus Plus (SIEMENS, Germany) to establish a radiation enteritis (RE) model.

Expression of phenyllactate dehydrogenase from *B. coccoides* in *E. coli* BL21 (DE3)

Using the NCBI BLAST alignment tool (v2.16), we identified the putative *fldH* gene in BC (DSM 935, WP_115622943.1) through alignment with the *fldH* gene of *C. sporogenes* ATCC 15579 (WP_003483291.1), which encodes a known phenyllactate dehydrogenase. The protein sequences of *fldH* from *C. sporogenes* and the putative *fldH* from BC (WP_115622943.1) were employed for predicting protein structures using the AlphaFold3 server (https://alphafoldserver.com/). The structural comparison of these proteins was performed using the US-align (v20241108) method. Visualization of the macromolecular structures was achieved through the PyMOL molecular graphics system (http://www.pymol.org/pymol, v3.2.0a).

Standard molecular cloning techniques were employed to clone the DNA fragments encoding the full-length *fldH* gene into the pET-28a (+) vector. Specifically, the *fldH* gene from BC was amplified from DNA extracts of BC bacterial cultures using a sense primer 5′-CGGATC-CATGGATAGGGAGGC-3′ incorporating an *BamHI* restriction site (underlined) and an antisense primer 5′-GCTCGAGTCATTTCAG-TATCC-3′ containing a *XhoI* site (underlined). The resulting PCR products were purified from agarose gel, digested with *BamHI* and *XhoI*, and subsequently cloned into pET-28a (Invitrogen) using the standard heat shock method. After overexpression of *fldH* in *E. coli* BL21 (Yeasen, 11804ES80), the bacteria were grown at 37 °C to an OD_{600} of 0.6. Afterwards, fldH protein expression was induced with 200 mM isopropyl-β-D-thiogalactopyranoside (IPTG) (Selleck, S6826) for 6 h at 37 °C. *E. coli* and *fldH*-overexpressing *E. coli* (*E. coli-fldH*) were incubated in brain heart infusion (BHI) medium (OXOID, CM1135B) for 24 h at 37 °C under aerobic conditions.

Fecal bacteria quantification

Fecal bacterial DNA was extracted using the TIANamp Stool DNA Kit (TIANGEN), and quantitative PCR (qPCR) was conducted with SYBR Green Real-time PCR Master Mix (TOYOBO). The quantification of BC, *P. russellii* and *C. sporogenes* was achieved through the use of standard curves, which were constructed from cloned DNA amplified with conserved specific primers (primers are detailed in the Supplementary Table 1).

Isolation of intestinal epithelial cells (IECs) and lamina propria mononuclear cells (LPMCs)

Murine IECs and LPMCs were obtained from the colon and ileum[40]. Briefly, the colon and ileum were longitudinally opened and cut into pieces. These pieces were then incubated with EDTA (5.5 mM) and dithiothreitol (DTT) (1 mM) in Hank's balanced salt solution. Following vortexing and passage through a 70 μm strainer, the suspension of IECs was washed twice by centrifugation at 600 × *g* for 3 min and collected for subsequent experiments. The remaining lamina propria tissue was further processed by incubating with a digestion solution containing collagenase (1 mg/mL) and DNase (0.2 mg/mL). The resulting LPMC suspension was subjected to Percoll-gradient separation and harvested for further analysis.

Quasi-targeted metabolomics

Metabolites were extracted from the colon tissues of mice after BC colonization and subsequently sent to BGI (Shenzhen, China) for targeted metabolomics analyzes. High-performance LC-MS/MS was used to perform high-sensitivity, wide-coverage, and high-throughput HM700-targeted quantification of 700 metabolites in these samples (https://www.bgi.com/global/service/hm700). In detail, appropriate amounts of experimental or quality control (QC) samples were resuspended in 140 μL of a 50% water/methanol solution, lysed, and centrifuged, and the supernatant was transferred to a new tube. A standard curve was prepared by serial dilution of an HM700 mixed standard. The experimental sample, QC sample, and standard were subjected to a derivatization reaction, and the resulting compounds were diluted in HM700 diluent and centrifuged at 12,000 × *g* at 4 °C for 10 min. The supernatant was applied to LC-MS/MS analysis on an LC-MS QTRAP 6500 Plus (SCIEX, USA). Chromatographic separation was performed on a BEH C18 column (2.1 × 100 mm, 1.7 μm; Waters). The mobile phases consisted of water containing 0.1% formic acid (solvent A) and acetonitrile containing 30% isopropanol (solvent B). Chromatographic separation was performed on a BEH C18 column (2.1 mm × 100 mm, 1.7 μm; Waters). Elution was carried out using the following linear gradient: 0–1.00 min, 5% B; 1.00–5.00 min, 5–30% B; 5.00–9.00 min, 30–50% B; 9.00–11.00 min, 50–78% B; 11.00–13.50 min, 78–95% B; and 13.50–14.00 min, 95–100% B, at a flow rate of 0.400 mL/min. The column was then washed at 100% B from 14.00 to 16.00 min at a flow rate of 0.600 mL/min, followed by re-equilibration at 5% B from 16.00 to 18.00 min at a flow rate of 0.400 mL/min. The column temperature was maintained at 40 °C. Mass spectrometric analysis was performed using an electrospray ionization source operated in both positive and negative ion modes (ESI+ and ESI−). The ion source parameters were set as follows: ion source temperature, 400 °C; ion spray voltage, 4500 V in positive mode and −4500 V in negative mode; ion source gas 1 (GS1), ion source gas 2 (GS2), and curtain gas (CUR) were set to 60, 60, and 35 psi, respectively. Data acquisition was conducted in multiple reaction monitoring (MRM) mode using a targeted MRM method that included precursor–product ion transitions, collision energy (CE), declustering potential (DP), and retention time information for each target metabolite. Skyline software (v24.1) was utilized to identify and qualify the metabolites for each sample, using the following parameters: "Mass: Monoisotopic peaks, Mass Tolerance: 0.6 Da, Mass Range: 50–1500 Da." Subsequently, probabilistic quotient normalization and quality control-robust spline signal correction based on QC samples were applied to the metabolomic profile using the *metaX* R package (v1.4.2). Classification and functional annotation of metabolites were performed based on the Human Metabolome Database and the KEGG database. Partial least squares discrimination analysis (PLS-DA) was employed to identify differentially abundant metabolites between groups, utilizing the '*opls*' function with parameter "orthoI=0" from the *ropls* R package (v1.34). Metabolites with a Variable Importance in Projection score >1 and an absolute log2-transformed fold change >1 were considered differentially abundant. KEGG pathway enrichment analysis was performed using the *ClusterProfiler* R package (v4.14.6)[41], based on KEGG compound-pathway relationships (http://rest.kegg.jp/link/pathway/compound). The metabolite profiles are provided in Supplementary Data 3.

Tryptophan-targeted metabolomics

Metabolites were extracted from BC supernatant samples and subsequently sent to BGI (Shenzhen, China) for tryptophan-targeted metabolomics analysis. Ultra-performance LC-MS was employed to quantify 29 tryptophan-related metabolites in these samples (https://www.bgi.com/global/service/targeted-metabolomics). Sample extracts were analyzed using a Waters UPLC I-Class Plus system (Waters, USA) coupled with a QTRAP 6500 Plus mass spectrometer (SCIEX, USA). Chromatographic separation was performed on an HSS T3 column (1.8 μm, 2.1 × 100 mm, Waters). The mobile phases consisted of water containing 0.01% formic acid and 5 mM ammonium acetate (A) and acetonitrile containing 0.02% formic acid (B). The gradient elution program was as follows: 0–7 min, 5% B; 7–9 min, 40% B; 9–10.6 min, 95% B; and 10.6–13 min, 5% B for column re-equilibration. The flow rate was 0.35 mL/min, the injection volume was 3 μL, and the column temperature was maintained at 40 °C. Mass spectrometric detection

was performed using a Turbo Ion Spray source operated in both positive and negative ion modes. The ion source temperature was set to 550 °C. Ion spray voltage was set to +5000 V in positive mode and −4500 V in negative mode. Gas 1 (GS1), gas 2 (GS2), and curtain gas (CUR) were set at 55, 55, and 30 psi, respectively. Quantification was conducted in MRM mode with optimized parent-daughter ion pairs and retention times for each target metabolite. Collision energy (CE) and declustering potential (DP) parameters were optimized individually based on analyte characteristics. Data acquisition and quantification were performed using MultiQuant software (SCIEX, USA, v3.0.2). The resulting data matrix, containing metabolite identification and quantitative information, was exported for further analysis. Subsequent data processing was conducted in *metaX* package. Missing values were imputed by replacing them with a small random number between 0.000001 and 0.000005. All other values represent absolute quantitative measurements, and no normalization was applied. Differences between BC supernatant and control (CMC) were assessed using a two-sided Welch's *t*-test, followed by Benjamini–Hochberg (BH) correction for multiple comparisons. The profile of tryptophan-related metabolites in the supernatant of BC and the control is presented in Supplementary Data 4.

DNA extraction, 16S rDNA amplicon sequencing and data analyses

Fecal samples (~200 mg) were resuspended in Qiagen's ASL buffer and homogenized for 2 min. Total fecal DNA was extracted from the resulting supernatant using a QIAamp DNA Stool Mini Kit (Qiagen, Germany), and DNA concentration and purity were measured by Qubit (Thermo Fisher Scientific, USA). The stool DNA was then amplified using Phusion High-Fidelity PCR Master Mix (New England Biolabs, USA) by PCR targeting the variable regions 3 and 4 (V3–V4) of the 16S rDNA, employing a pair of primers 338F (5′-ACTCCTACGGGAGGCAGCA-3′) and 806R (5′-GGACTACHVGGGTWTCTAAT-3′). Multiplex sequencing of amplicons with sample-specific barcodes was performed using the MiSeq Illumina platform (Guangdong Meg Gene Biotechnology Co., Ltd, China). The sequences were analyzed using the QIIME2 platform (v2023.05, https://qiime2.org/). Reads were quality filtered, denoised, and merged into amplicon sequence variants using DADA2 with default parameters. Taxonomic assignment was conducted using the feature-classifier plugin in QIIME2, referencing the SILVA (v138) database. The Wilcoxon rank-sum test was used to measure significant differences in the relative abundance of microbial taxa between patients and healthy controls. Additionally, we used both Linear Discriminant Analysis Effect Size (LEfSe) and a random forest model to confirm the enrichment direction of specific genera. These analyzes were performed in R environment (v4.4) using the *microeco* (v1.8), *randomForest* (v4.7), and *pROC* (v1.18) packages.

β-Hydroxybutyrate (BHB) analysis

Bacteria culture supernatant samples and cIECs from murine models were collected for BHB measurement. cIEC pellets harvested from colon tissues (~7 cm) were homogenized with sterile grinding beads in 500 µL PBS at 45 Hz for 1 min, centrifuged (6000 × *g*, 5 min, 4 °C) to collected the supernatant and divided in two aliquots for total protein and BHB measurement. Levels of BHB were normalized to the total protein content. Total protein was measured by BCA Protein Assay Kit (EpiZyme, ZJ101), and BHB level was determined by BHB Assay Kit (Solarbio, BC5085) following the manufacturer's instructions.

Flow cytometry analysis

1×10^6 cLPMCs were incubated with 1 mg of anti-CD16/32 antibody (BioLegend, 101320) for 10 min to block non-specific binding of immunoglobulin to the Fc receptors. Subsequently, cells were stained for live cells using the Live/Dead Fixable Aqua Dead Cell Stain Kit (BD Biosciences, 564995) for 30 min. Following this, the appropriate amount of pre-diluted fluorescent-labeled antibodies (eBioscience, 11-0032-82, 48-0041-82, 11-9668-80; MultiSciences, F41011b04, F21480A02; Tonbo Biosciences, 20-0081; BioLegend, 117309) was added to each tube as per the manufacturer's recommendations. The cells were then incubated in the dark at 4 °C for 30 min and washed twice with PBS. Flow cytometry was conducted using the FACSVerse system (BD Biosciences) with FSC and SSC thresholds set at 1000 and a logarithmic scale. Between 30,000 and 150,000 events were recorded and analyzed using FlowJo software (Tree Star). The flow cytometry experiments, including the complete sequential FACS gating strategy, were performed as an integral part of the same methodological pipeline. The detailed sequential gating strategy used for all flow cytometry data is illustrated in Supplementary Fig. 1h of our companion paper (Zhang et al., *Nature Communications*, 2026, https://doi.org/10.1038/s41467-026-69341-z).

Isolation of crypts, culture of intestinal organoids and treatments

For murine organoid culture: colon tissues of mice were removed, wash with cold PBS, opened longitudinally, cut into pieces and then incubated on ice in buffer (1× PBS, 8 mM EDTA, 0.5 mM DTT) for 20-45 min. Crypts were then mechanically separated from the connective tissue by shaking, and filtered through a 70 µm mesh into a 50 mL conical tube to remove villus material and tissue fragments. Isolated crypts were centrifuged for 2 min at 68 × *g*, resuspended in organoid growth medium for organoid culture.

Murine colonic organoids were cultured from isolated crypts[42]. Briefly, isolated crypts were centrifuged for 2 min at 68 × *g*, resuspended in the appropriate volume of cold mouse colonic organoid growth medium (bioGenous, K2204-MC) and embedded in equal volume of Matrigel matrix (ABW, 082703) at 50-250 crypts/20-30 µL in a 48-well plate. The crypts/Matrigel mixture was allowed to solidify for 15–20 min in a 37 °C incubator and then overlaid with additional 200 µL organoid growth medium. After 4-day culture, organoids were dissociated in organoid dissociation solution (bioGenous, E238001) for 2 min at 37 °C according to the manufacturer's protocol, centrifuged at 68 × *g* for 2 min, resuspended in organoid culture medium, and cultured as described above for organoids passaging. After culture for 48 h, 100 µM ILA or IPA was added to organoids and incubated at 37 °C for 6 h. For the BHB pretreatment, 10 mM BHB was added to organoids and incubated at 37 °C for 3 h. To establish pathological conditions for inflammation, IFN-γ/TNF-α (20 ng/mL each) was added for 6 h or 18 h.

For human organoid culture: adult human organoids were prepared from endoscopy samples obtained from non-IBD individuals. Crypts isolation and organoid culture methods are consistent with mice. Human colonic organoid kit (K2003-HC, bioGenous) was used for human organoid growth medium. At day 3, 200 µM ILA/IPA and 10 mM BHB were added to organoids and incubated at 37 °C for 6 h or 3 h. To establish pathological conditions for inflammation, IFN-γ/TNF-α (187.5 ng/mL each) were added for 6 h, 24 h or 48 h.

RNA extraction, library construction, sequencing, and data analyses

Total RNA was extracted from bulk cIECs isolated from mice using TRIzol reagent (Invitrogen, USA). A library was constructed using the ALFA-SEQ RNA Library Prep Kit, following the manufacturer's instructions. Sequencing was performed on an Illumina NovaSeq 6000 platform, producing paired-end reads of 150 bp. The raw reads were filtered to remove unqualified reads using fastp (v0.23.2) software with default settings. The filtered reads were then mapped to the mouse reference genome (GRCm39) using HISAT2 (v2.2.1)[43]. Transcript assembly, gene-mapped read counts, and fragments per kilobase of exon model per million mapped fragments (FPKM) values were generated using StringTie (v3.0.0)[44]. The resulting FPKM profiles were

then used as input for *limma* (v3.62.2)[45]. GO and KEGG pathway enrichment analyzes were conducted using the *ClusterProfiler* package in the R environment (v4.4).

Collection and analysis of public metabolomic and metagenomic datasets

The feature table of the amplicon-based metagenomic dataset from the study by Lloyd-Price et al. was obtained from the Inflammatory Bowel Disease Multi-omics Database (IBDMDB, https://ibdmdb.org/). The analytical methodology employed for this dataset was similar to that described above. Meanwhile, several shotgun metagenomic datasets were downloaded for re-analysis using a reference-based method. Raw sequencing reads from all samples underwent quality control using fastp. Reads were discarded if they contained more than 55 bases with quality scores below 20, more than 5 ambiguous bases ('N'), or exhibited low complexity or adapter contamination. Human-derived reads were removed by mapping against the human reference genome (GRCh38) using Bowtie2 (v2.5.4). We mapped the high-quality metagenomic reads from all samples to the genomes of *B. coccoides* strain DSM 935, *C. sporogenes* strain ATCC 15579 and *P. russellii* strain RT-10B using Minimap2 (v2.26-r1175) with an alignment identity >95%. Read counts mapped to each genome were normalized by total reads per sample. The two-sided Wilcoxon rank-sum test with BH adjustment for multiple comparisons was employed to assess significant differences in the relative abundance of *B. coccoides*. Spearman's rank correlation was used to assess associations among *B. coccoides*, *C. sporogenes*, and *P. russellii* based on their relative abundances across multiple datasets.

Quantitative real-time PCR

Total RNA from bead-homogenized tissue samples or cell culture was extracted using FreeZol reagent (Vazyme, R711) following the manufacturer's instructions. PCR reactions were performed with HiScript II One Step qRT-PCR SYBR®Green Kit (Vazyme) on a Gentier 96R Real-Time PCR System (TIANLONG, Xi'an, China). Transcript levels of the indicated genes were normalized to endogenous control GAPDH for each individual sample using the specific primers listed in the Supplementary Table 1 and quantified using the comparative critical threshold cycle $2^{-\Delta\Delta CT}$ method.

Western blotting

Cells and tissue homogenates were lysed in RIPA buffer containing protease and phosphatase inhibitors. Total proteins were quantified by BCA Protein Assay Kit, separated on 10% sodium dodecyl sulfate-polyacrylamide gel electrophoresis (SDS-PAGE), and then transferred onto polyvinylidene difluoride membranes (BioRad). The membrane was blocked in blocking buffer (5% BSA in 1 × TBST, Tris-buffered saline and Tween-20) and then incubated with primary antibodies overnight at 4 °C. After incubation, the membrane was washed three times with TBST and incubated with horseradish peroxidase (HRP)-conjugated secondary antibodies. The membrane was washed four times in TBST and visualized using an enhanced chemiluminescence kit (Vazyme, E423-01/02) with a ChemiDoc Touch Gel Imaging System (Bio-Rad). Uncropped and unprocessed scans of all Western blots are provided in the Source Data file.

Tissue histology and immunostaining

Colon 'Swiss rolls' soaked in 4% paraformaldehyde solution were dehydrated, embedded in paraffin, cut into 4 μm thick sections, and stained with haematoxylin and eosin (H&E) using standard procedures. Slices were evaluated by an experienced pathologist in a blinded manner, and histological scores were assessed based on the following parameters according to previous research: inflammation, epithelial defects, crypt atrophy, dysplasia/neoplasia, and the area affected by dysplasia[22]. For the staining of goblet cells, colon sections were also stained in Alcian blue for 10 to 15 min and dehydrated in 100% alcohol and xylene.

For immunofluorescence (IFA) analysis, deparaffinized colon sections were blocked with 10% normal goat serum for 10 min at room temperature. The slides were then incubated with specific primary antibodies at 4 °C overnight. Antibodies used: anti-IL-6 (1:50, Proteintech, 21865-1-AP), anti-occludin (1:100, Proteintech, 13409-1-AP), anti-Muc2 (1:100, Proteintech, 27675-1-AP), anti-Ki67 (1:250, Abcam, ab16667), anti-LGR5 (1:400, Affinity, DF2816), anti-Phospho-STAT1 (1:200, MCE, HY-P80856) and anti-HOPX (1:100, ABclonal, A15537). After washing with PBS for three times, the slides were then incubated with fluorescently labeled secondary antibodies (Jackson ImmunoResearch) for additional 2 h at room temperature in dark, and nuclei were stained with DAPI (Roche, Switzerland). TUNEL staining was performed using the In situ Cell Death Detection POD kit (Roche Diagnostics) on the Discovery XT according to the manufacturer's protocol. All analyzes were performed using ImageJ software.

Evaluating bacterial cross-feeding in vitro

BC (5×10^6 CFU) was co-cultured with either *P. russellii* or *C. sporogenes* (5×10^6 CFU each) in Cooked Meat medium under anaerobic conditions at 37 °C for 12 h. After incubation, genomic DNA was extracted from co-culture samples using the EasyPure Stool Genomic DNA Kit (TransGen Biotech). Bacterial abundances were absolutely quantified using digital PCR (dPCR) on the QIAcuity system (QIAGEN) with species-specific primers (primers are detailed in the Supplementary Table 1). Each 40 μL dPCR reaction consisted of 1× EvaGreen PCR Master Mix (QIAGEN), 400 nM of each primer, and ~100 ng of DNA template. The reaction mixture was automatically partitioned into ~26,000 nanowells using the QIAcuity One platform. Thermal cycling was performed as follows: 95 °C for 2 min; 40 cycles of 95 °C for 15 s, 50–60 °C for 15 s, and 72 °C for 15 s; followed by a final extension at 40 °C for 5 min. Fluorescence signal acquisition was conducted in-plate using the QIAcuity One instrument. Absolute quantification of target DNA copies was automatically calculated by the QIAcuity Software Suite through binary fluorescence thresholding.

Evaluating bacterial cross-feeding in vivo

Female C57BL/6 J mice (6–8 weeks old) were maintained under standard conditions. Mice ($n = 5$ per group) were orally administered 1×10^9 CFU of BC suspended in phosphate-buffered saline (PBS) on days 0 and 2. Control mice received an equal volume of PBS. All mice were euthanized on day 4, and cecal contents were collected for microbial analysis.

GF mice were divided into six groups ($n = 6$ per group). On days −4 and −2, respective groups received oral gavage of the following bacterial suspensions in 150 μL of sterile anaerobic PBS: BC (1×10^6 CFU); *P. russellii* (1×10^6 CFU); *C. sporogenes* (1×10^6 CFU); a combination of BC and *P. russellii* (5×10^5 CFU each); or BC and *C. sporogenes* (5×10^5 CFU each). Fecal samples were collected on day 0 for DNA extraction, followed by a 3-day DSS colitis induction.

Genomic DNA was extracted from colonic contents using the EasyPure Stool Genomic DNA Kit (TransGen Biotech). Quantitative PCR (qPCR) was performed using a LightCycler 480 II system (Roche) with 2× RealStar Fast SYBR qPCR Mix (Genstar), in accordance with the manufacturer's instructions. The thermocycling protocol included an initial denaturation at 95 °C for 5 min, followed by 45 cycles of 95 °C for 10 s, 50 °C for 10 s, and 72 °C for 10 s. The relative abundance of each target bacterium was quantified using the $2^{-\Delta\Delta Ct}$ method, normalized to the 16S rRNA gene.

Quantitative analysis of ILA, IPA and tryptophan

To prepare culture supernatant for ultrahigh-performance liquid chromatography-tandem mass spectrometry (UHPLC-MS/MS)

analysis, proteins were precipitated by mixing 100 µL of sample with 900 µL of methanol to improve the chromatographic baseline. After thorough vortex-mixing, samples were incubated at −20 °C for 2 h and centrifuged at 10,000 × *g* for 10 min at 4 °C. Then, 100 µL of the supernatant was diluted to 1 mL with water, vortex-mixed, filtered, and subjected to UHPLC-MS/MS analysis. For caecal content samples, ~100 mg of samples was resuspended in 1 mL of 80% methanol, homogenized by vortexing, and sonicated for 30 min. After centrifugation at 10,000 × *g* for 10 min at 4 °C, the supernatant was collected, filtered, and analyzed via UHPLC-MS/MS.

UHPLC-MS/MS analysis was performed using a Vanquish UHPLC system (Thermo Fisher Scientific, USA) coupled to an Orbitrap Q Exactive™ HF mass spectrometer (Thermo Fisher Scientific, USA). Separation was carried out on a Hypesil Gold column (100 × 2.1 mm, 1.9 µm) with a 15 min linear gradient at a flow rate of 0.2 mL/min. The mobile phase consisted of 0.1% formic acid in water (eluent A) and 0.1% formic acid in acetonitrile (eluent B). The gradient program was set as follows: 10% B (0–1.5 min), 10-34% B (1.5–6 min), 34–90% B (6–9 min), 90–10% B (9–13.5 min), and 10% B (13.5–15 min). The column temperature was maintained at 40 °C. Mass spectrometry detection was conducted in positive ion mode with the following parameters: spray voltage 3.2 kV, capillary temperature 320 °C, sheath gas flow rate 40 arb, and auxiliary gas flow rate 10 arb.

Individual stock solutions of indole lactic acid (ILA), indole propionic acid (IPA), and tryptophan (Trp) were prepared at 1 mg/mL in methanol and stored at −80 °C until use. Individual calibration curves were generated for each analyte. Seven calibration standards were prepared by serial dilution for each compound across its respective concentration range of 0.005–10 µg/mL. Raw data acquired from UHPLC-MS/MS were processed using Compound Discoverer 3.1 (Thermo Fisher Scientific, USA). The processing workflow included peak alignment, peak picking, and quantitation. Peak areas were integrated using Xcalibur Qual Browser (Thermo Fisher Scientific, USA) with manual review to ensure accuracy. Peak intensities were normalized to total spectral intensity to correct for sample-to-sample variation. Molecular formulas were predicted from high-resolution MS data by evaluating additive ions, molecular ion peaks, and fragment ions. Compound identities were confirmed by matching experimental spectra against reference spectra in the mzCloud (https://www.mzcloud.org/), mzVault, and MassList databases. Quantification of ILA, IPA, and tryptophan was performed using external calibration curves. The UHPLC-MS/MS analysis demonstrated excellent linearity for IPA, ILA and Trp across a broad concentration range, as detailed in Supplementary Data 5.

Statistics and reproducibility

GraphPad Prism was used for all statistical analyzes. Representative H&E and immunofluorescent staining are presented. Error bars represent mean ± standard deviation (SD) in all figures, and differences between groups were analyzed by two-sided Student's *t*-tests, one-way ANOVA followed by Tukey's post hoc test for multiple comparisons, and Spearman's rank correlation analysis. The demographic characteristics were analyzed using the Chi-squared test and the two-sided Welch *t*-test to determine if there were any significant differences between the CD and healthy groups. Experimental sample numbers (n) are shown in the figure legends. $P < 0.05$ was considered to indicate statistical significance.

Sample sizes (typically 3–6 biological replicates per group) were selected based on established standards in the field and our preliminary data, which indicated that this range was sufficient to detect biologically relevant effects. No statistical method was used for prior sample size calculation. All data generated were included in the analyzes, with no exclusions. For animal studies, mice were randomly assigned to experimental groups. Key experimental findings were independently replicated at least three times with consistent results.

Reporting summary

Further information on research design is available in the Nature Portfolio Reporting Summary linked to this article.

Data availability

The 16S rRNA amplicon sequencing data and raw bulk RNA sequencing data generated in this study have been deposited in the Genome Sequence Archive (GSA) in National Genomics Data Center (NGDC) under accession codes CRA018493 and CRA018487, respectively. The fecal metabolomic profiles and tryptophan-related metabolite profiles generated in this study are provided in the Supplementary Data 3 and 4. The feature table of the amplicon-based metagenomic dataset from the study by Lloyd-Price et al. was obtained from the Inflammatory Bowel Disease Multi-omics Database (IBDMDB, https://ibdmdb.org/). The raw metagenomic datasets analyzed in this study were obtained from the previously published studies and are publicly available at European Nucleotide Archive under the following project accessions: PRJEB15371 (HeQ_2017), PRJNA385949 (HallAB_2017), PRJNA398089 (LloydPriceJ_2019), PRJNA389280 (SchirmerM_2018), PRJNA429990 (WengY_2019), PRJEB67456 (YanQ_2023c). The genome sequence and annotation files for *Mus musculus* (GRCm39, release 110) were downloaded from the Ensembl database. The genome sequences of *Homo sapiens* were download from NCBI database with accession code GCF_000001405.40. The genome, coding, and protein sequences of *Clostridium sporogenes* strain ATCC 15579, *Peptostreptococcus russellii* strain RT-10B and *Blautia coccoides* strain DSM 935 were downloaded from the NCBI database under accession numbers GCF_000155085.1, GCF_003012055.1 and GCF_034355335.1, respectively. Source data are provided with this paper.

Code availability

The intermediate results, analysis and visualization codes used in this study have been uploaded into the GitHub repository, accessible at https://github.com/mengjx855/25-BC-IPA-ISC.

References

1. Miyoshi, H., Ajima, R., Luo, C. T., Yamaguchi, T. P. & Stappenbeck, T. S. Wnt5a potentiates TGF-beta signaling to promote colonic crypt regeneration after tissue injury. *Science* **338**, 108–113 (2012).
2. Barker, N. et al. Identification of stem cells in small intestine and colon by marker gene Lgr5. *Nature* **449**, 1003–1007 (2007).
3. Wu, N. et al. MAP3K2-regulated intestinal stromal cells define a distinct stem cell niche. *Nature* **592**, 606–610 (2021).
4. Wang, R. et al. Gut stem cell necroptosis by genome instability triggers bowel inflammation. *Nature* **580**, 386–390 (2020).
5. Villablanca, E. J., Selin, K. & Hedin, C. R. H. Mechanisms of mucosal healing: treating inflammatory bowel disease without immunosuppression? *Nat. Rev. Gastroenterol. Hepatol.* **19**, 493–507 (2022).
6. Montgomery, R. K. et al. Mouse telomerase reverse transcriptase (mTert) expression marks slowly cycling intestinal stem cells. *Proc. Natl. Acad. Sci. USA* **108**, 179–184 (2011).
7. Powell, A. E. et al. The pan-ErbB negative regulator Lrig1 is an intestinal stem cell marker that functions as a tumor suppressor. *Cell* **149**, 146–158 (2012).
8. Yan, K. S. et al. The intestinal stem cell markers Bmi1 and Lgr5 identify two functionally distinct populations. *Proc. Natl. Acad. Sci. USA* **109**, 466–471 (2012).
9. Takeda, N. et al. Interconversion between intestinal stem cell populations in distinct niches. *Science* **334**, 1420–1424 (2011).

10. Tao, S. et al. Wnt activity and basal niche position sensitize intestinal stem and progenitor cells to DNA damage. *EMBO J.* **36**, 2920–2921 (2017).
11. Metcalfe, C., Kljavin, N. M., Ybarra, R. & de Sauvage, F. J. Lgr5+ stem cells are indispensable for radiation-induced intestinal regeneration. *Cell Stem Cell* **14**, 149–159 (2014).
12. Wang, Y. et al. Long-term culture captures injury-repair cycles of colonic stem cells. *Cell* **179**, 1144–1159 e1115 (2019).
13. Stewart, A. S. et al. HOPX(+) injury-resistant intestinal stem cells drive epithelial recovery after severe intestinal ischemia. *Am. J. Physiol. Gastrointest. Liver Physiol.* **321**, G588–G602 (2021).
14. Ayyaz, A. et al. Single-cell transcriptomes of the regenerating intestine reveal a revival stem cell. *Nature* **569**, 121–125 (2019).
15. Pull, S. L., Doherty, J. M., Mills, J. C., Gordon, J. I. & Stappenbeck, T. S. Activated macrophages are an adaptive element of the colonic epithelial progenitor niche necessary for regenerative responses to injury. *Proc. Natl. Acad. Sci. USA* **102**, 99–104 (2005).
16. Kaiko, G. E. et al. The colonic crypt protects stem cells from microbiota-derived metabolites. *Cell* **167**, 1137 (2016).
17. Peck, B. C. E., Shanahan, M. T., Singh, A. P. & Sethupathy, P. Gut microbial influences on the mammalian intestinal stem cell niche. *Stem Cells Int.* **2017**, 5604727 (2017).
18. Manichanh, C., Borruel, N., Casellas, F. & Guarner, F. The gut microbiota in IBD. *Nat. Rev. Gastroenterol. Hepatol.* **9**, 599–608 (2012).
19. Shan, Y., Lee, M. & Chang, E. B. The gut microbiome and inflammatory bowel diseases. *Annu. Rev. Med.* **73**, 455–468 (2022).
20. Abdulla, A., Awla, D., Thorlacius, H. & Regner, S. Role of neutrophils in the activation of trypsinogen in severe acute pancreatitis. *J. Leukoc. Biol.* **90**, 975–982 (2011).
21. Wang, G. et al. Ginsenoside Rg3 enriches SCFA-producing commensal bacteria to confer protection against enteric viral infection via the cGAS-STING-type I IFN axis. *ISME J.* **17**, 2426–2440 (2023).
22. Zhang, Y. et al. Dubosiella newyorkensis modulates immune tolerance in colitis via the L-lysine-activated AhR-IDO1-Kyn pathway. *Nat. Commun.* **15**, 1333 (2024).
23. Subramanian, B. C. Inflammatory bowel disease: DCs sense LTB(4) to drive T(H)1 and T(H)17 differentiation. *Cell Mol. Immunol.* **17**, 307–309 (2020).
24. Gregorieff, A., Liu, Y., Inanlou, M. R., Khomchuk, Y. & Wrana, J. L. Yap-dependent reprogramming of Lgr5(+) stem cells drives intestinal regeneration and cancer. *Nature* **526**, 715–718 (2015).
25. Richmond, C. A. et al. JAK/STAT-1 signaling is required for reserve intestinal stem cell activation during intestinal regeneration following acute inflammation. *Stem Cell Rep.* **10**, 17–26 (2018).
26. Zhang, Y. et al. Microbiota-derived IPA protects against colitis by regulating intestinal HMGCS2-mediated ketogenesis to facilitate mucosal healing. *Nat Commun.* https://doi.org/10.1038/s41467-026-69341-z (2026).
27. Agus, A., Planchais, J. & Sokol, H. Gut microbiota regulation of tryptophan metabolism in health and disease. *Cell Host Microbe* **23**, 716–724 (2018).
28. Li, Y. et al. Exogenous stimuli maintain intraepithelial lymphocytes via aryl hydrocarbon receptor activation. *Cell* **147**, 629–640 (2011).
29. Holmberg, S. M. et al. The gut commensal Blautia maintains colonic mucus function under low-fiber consumption through secretion of short-chain fatty acids. *Nat. Commun.* **15**, 3502 (2024).
30. Cheng, C. W. et al. Ketone body signaling mediates intestinal stem cell homeostasis and adaptation to diet. *Cell* **178**, 1115–1131 e1115 (2019).
31. Terranova, C. J. et al. Reprogramming of H3K9bhb at regulatory elements is a key feature of fasting in the small intestine. *Cell Rep.* **37**, 110044 (2021).
32. Roda, G., Jharap, B., Neeraj, N. & Colombel, J. F. Loss of response to anti-TNFs: definition, epidemiology, and management. *Clin. Transl. Gastroenterol.* **7**, e135 (2016).
33. Dahmus, J., Rosario, M. & Clarke, K. Risk of lymphoma associated with anti-TNF therapy in patients with inflammatory bowel disease: implications for therapy. *Clin. Exp. Gastroenterol.* **13**, 339–350 (2020).
34. Singh, S., Facciorusso, A., Dulai, P. S., Jairath, V. & Sandborn, W. J. Comparative risk of serious infections with biologic and/or immunosuppressive therapy in patients with inflammatory bowel diseases: a systematic review and meta-analysis. *Clin. Gastroenterol. Hepatol.* **18**, 69–81 e63 (2020).
35. Sinha, A. K. et al. Dietary fibre directs microbial tryptophan metabolism via metabolic interactions in the gut microbiota. *Nat. Microbiol.* **9**, 1964–1978 (2024).
36. Kitada, Y. et al. Bioactive polyamine production by a novel hybrid system comprising multiple indigenous gut bacterial strategies. *Sci. Adv.* **4**, eaat0062 (2018).
37. Jia, D. et al. Microbial metabolite enhances immunotherapy efficacy by modulating T cell stemness in pan-cancer. *Cell* **187**, 1651–1665 e1621 (2024).
38. Babickova, J. et al. Sex differences in experimentally induced colitis in mice: a role for estrogens. *Inflammation* **38**, 1996–2006 (2015).
39. Tshikudi, D. M., Bernstein, C. N., Mishra, S., Ghia, J. E. & Armstrong, H. K. Influence of biological sex in inflammatory bowel diseases. *Nat. Rev. Gastroenterol. Hepatol.* **22**, 415–437 (2025).
40. Weigmann, B. et al. Isolation and subsequent analysis of murine lamina propria mononuclear cells from colonic tissue. *Nat. Protoc.* **2**, 2307–2311 (2007).
41. Xu, S. et al. Using clusterProfiler to characterize multiomics data. *Nat. Protoc.* **19**, 3292–3320 (2024).
42. Sato, T. et al. Single Lgr5 stem cells build crypt-villus structures in vitro without a mesenchymal niche. *Nature* **459**, 262–265 (2009).
43. Kim, D., Paggi, J. M., Park, C., Bennett, C. & Salzberg, S. L. Graph-based genome alignment and genotyping with HISAT2 and HISAT-genotype. *Nat. Biotechnol.* **37**, 907–915 (2019).
44. Pertea, M. et al. StringTie enables improved reconstruction of a transcriptome from RNA-seq reads. *Nat. Biotechnol.* **33**, 290–295 (2015).
45. Ritchie, M. E. et al. limma powers differential expression analyses for RNA-sequencing and microarray studies. *Nucleic Acids Res.* **43**, e47 (2015).

Acknowledgements

We thank Dr. Daqian Xu, Dr. Dingjiacheng Jia and Dr. Yuhao Wang for their valuable comments for the manuscript. We appreciate Dr. Bin Zhou from Institute of Biochemistry and Cell Biology, Shanghai Institutes for Biological Sciences, Chinese Academy of Sciences for providing *Hopx-CreERT2* mice. The professional editing service NB Revisions was used for technical preparation of the text prior to submission. This work is supported by grants from the National Natural Science Foundation of China (No. 323B2007, No. 82174467, No. 82572567, No. 82574811 and No. 32471329) to Y.Z., S.J.Z., L.Z., and H. C.

Author contributions

S.J.Z., H.C., and Y.Z. designed the experiments. Y.Z., S.T., L.M., X.Z., J.G., J.W., and W. X. performed the experiments. J.M. conducted bioinformatics analysis. L.Z. collected samples and data. S.C coordinated the project. L.Z. and H.C. commented on and revised drafts of the manuscript. S.J.Z., Y.Z., S.T., J.M., and H.C. wrote the paper. S.J.Z. supervised research, coordination, and strategy.

Competing interests

The authors declare no competing interests.

Additional information

Supplementary information The online version contains supplementary material available at https://doi.org/10.1038/s41467-026-70062-6.

Correspondence and requests for materials should be addressed to Hairong Cheng, Li Zhang or Shu Jeffrey Zhu.

Peer review information *Nature Communications* thanks Philip Busbee, and the other, anonymous, reviewers for their contribution to the peer review of this work. A peer review file is available.